THESIS FOR THE DEGREE OF LICENTIATE OF ENGINEERING

Enhancements in Dielectric Response Characterization of Insulation Materials

Xiangdong Xu

High Voltage Engineering
Department of Material and Manufacturing Technology

CHALMERS UNIVERSITY OF TECHNOLOGY

Göteborg, Sweden 2013

Enhancements in Dielectric Response Characterization of Insulation Materials
XIANGDONG XU

道可道，非常道

Road signs show the usual way, but the best is changing

Abstract

The increasing demand of integrating various renewable energy recourses in power system requires extensive use of power electronic solutions, such as HVDC and FACTS, as these techniques allow energy conversion between different frequencies and serves to stabilize the network. Consequently, electric stresses other than traditional 50/60 Hz sinusoidal voltage stress are acting on high voltage insulation materials. Therefore, a need for fast and accurate characterization methods, which can be used to study the influence on insulation materials of different types of voltage waveforms, has arisen.

Dielectric response measurement is one commonly used non-destructive insulation test technique and has more than 100 years of history. Limitations like precision of the testing voltage waveform, high demand on a stable testing environmental condition, intricate specimen-electrode preparation, severe electrode geometric influences, etc., are however restraining the use of such measurements. In this project, several methods that are based on the Arbitrary Waveform Impedance Spectroscopy (AWIS) technique have been developed to enable fast and more accurate solid dielectric characterization.

A test setup that is based on the AWIS technique can be optimized by implementing several techniques such as voltage divider, voltage follower, shielding box, etc., to reduce the measurement noise and to avoid crosstalk between adjacent signals.

By utilizing optimized harmonic limited waveforms in the AWIS test setup, dielectric responses over a wide frequency spectrum can be determined simultaneously without degradation by signal aliasing. This also enables monitoring of the dielectric properties under fast changing test conditions as a source of systematic error is eliminated when all frequencies are obtained at the same time and at the same conditions.

An air reference method and a contact-free electrode arrangement are described in this work to enhance the dielectric characterization accuracy by avoiding contact problems at the electrodes. It is shown that by performing a calibration with electrode gap filled with air under the same conditions as the material is tested, the air reference method can improve the measurement accuracy substantially. This type of approach also eliminates the need of a detailed model of the analog measurement circuit. In conjunction with the contact-free measurements, the approach allows for avoiding complicated and time-consuming specimen preparation procedures. The measurement methodology as well as the electrode arrangement and error estimation are presented and evaluated using different dielectric response instruments and materials.

To improve the accuracy of dielectric permittivity, two methods are suggested in this work by either compensating or shielding the electrode setup from undesired geometric influences. One approach is to estimate a correction factor from a finite element method (FEM) model to improve the accuracy. The other approach uses a shielding guard electrode to avoid the geometric influence on measurement. Measurements of several PET films are used as an example to illustrate the use of correction factors in the application of contact free measurement. The latter method is only verified in FEM calculation.

Keywords: Dielectric characterization, frequency domain spectroscopy, harmonic limited waveform, contact-free electrode, air reference method, geometric corrections.

Acknowledgments

I am very grateful to my examiner Prof. Stanislaw Gubanski for providing excellent overview, consistent support and carefully revising all my manuscripts. My supervisor Prof. Tord Bengtsson, have shared his great expertise, teaching me the philosophy of research and life in general. He has always been ready for discussing any new issues and sharing valuable ideas. Through his continued guidance and encouragements, measurements become games and writing becomes confidence. My other supervisor Assoc. Prof. Jörgen Blennow has continuously served as an inspiration for both my master and PhD studies. In addition, we have shared interesting discussions concerning world, history, collections, and food throughout the years at Chalmers. My predecessor of this project Dr. Björn Sonerud is thanked for providing such an excellent platform, AWIS.

The reference group members are acknowledged for providing great source of ideas and support.

Colleagues from High Voltage Engineering group as well as division of Electric Power Engineering has helped to create a pleasant working atmosphere and with various matters. Fellows from KTH, Lund and Uppsala are also thanked for sharing valuable ideas and discussions during conferences and courses.

My parents, Chengqing Xu and Qingru Xiang are sincerely thanked for all the supports and encouragements, you are the ones who led me the person I am today. At last, but not least, my wife, Yu Liu, is specially thanked for all her love, understanding, and support to make a wonderful place called home.

Xiangdong Xu

Göteborg, Sweden

February, 2013

Table of Contents

1 Introduction

Today, the need of sustainable electric power system solutions is at the top of strategic development agendas all over the world. To integrate renewable energy sources as well as to balance energy production and consumption, many installations contain power electronic solutions in combination with solid dielectric insulation systems. In such systems, the insulation is subjected to increasingly higher dielectric stress and in many cases to stresses at higher frequencies than the traditional power frequency. Therefore, there is a growing interest in methods of fast and accurate dielectric characterization also at high frequencies for material selection and development.

Dielectric response measurement is one of the two main non-destructive insulation test techniques in high voltage engineering, the other being partial discharge measurement. Dielectric response measurements are used both for material studies and insulation system diagnostics.

In the dielectric material studies, dielectric response measurements are often employed as a characterization method. Limitations like requirement of steady-state test environmental conditions, elaborate specimen-electrode preparations, geometric influences in the permittivity determinations, etc. are however obstructing the practical use of such measurements.

1.1 The project

The aim of this project is to use and further develop Arbitrary Waveform Impedance Spectroscopy (AWIS) technique as a tool for accurate and fast dielectric material characterization [4-6]. This goal is addressed by studying some particular methods. Proper test waveforms for fast AWIS dielectric studies with regard to frequency content and harmonic aliasing are determined, the air reference method is proposed to avoid specimen surface contact problem and a deeper error analysis of this approach is presented. Dielectric constant measurement errors due to electrode geometric influences are compensated by comparisons to a finite-element model.

AWIS uses a versatile voltage-current measurement technique for dielectric material studies. It can not only measure a dielectric response under voltages with a specified frequency, but is also capable of determining a broad dielectric spectrum from one measurement provided the test voltage is rich enough in harmonics.

One problem with dielectric response characterization is the measurement time resolution, too long measurement time requires stable test conditions to obtain reliable dielectric properties over the measured frequency spectrum and this is obstructing the use of material monitoring in rapidly changing environmental conditions. In this project, a method is suggested to select proper harmonic limited waveforms for AWIS setup to perform fast dielectric characterization as extremely harmonic-rich test signals limit the measurement accuracy due to aliasing. Another limitation in accurate dielectric characterization is the specimen-electrode contact as an elaborate specimen preparation process, which is often required to avoid poor surface contact. To simplify

the specimen preparation and to increase the accuracy, a contact-free electrode arrangement and a supplementing air reference method are suggested. Further, as the AWIS technique can use a capacitive shunt to measure currents, in contrast to most commercial instruments which are mainly using operational amplifiers, measurements are possible at higher frequencies. However, a drawback of a current shunt is that a non-negligible voltage is present at the measurement electrode. Consequently, capacitive coupling between electrodes and surroundings are introduced which affect the accuracy of permittivity determination. Two methods are suggested in this project to either compensate or shield the geometric influences.

1.2 Outline of the thesis

This thesis describes the methods studied that aim for fast and accurate determination of dielectric properties. In chapter 2: "Background", the principle of dielectric response measurement and its history are presented and the background of the AWIS technique is reviewed. Chapter 3: "Experimental setup" presents considerations involved in implementing the AWIS technique for dielectric response measurements. In chapter 4: "Harmonic limited waveform", a method to construct an effective waveform for fast dielectric characterization is presented. The contact-free dielectric characterization and its supplementing air reference measurement method are presented in chapter 5: "Air reference method". Chapter 6: "Geometric influence on permittivity" addresses the issue of obtaining an accurate permittivity value despite undesired influences from the surroundings.

1.3 List of publications

1: Xu, Xiangdong; Bengtsson, Tord; Blennow, Jörgen; Gubanski, Stanislaw, *Harmonic Limited Test Waveforms for Fast AWIS Dielectric Studies*, 22nd Nordic Insulation Symposium (NORDIS 11), June 13-15, Tampere, Finland, p. 199-202

2: Xu, Xiangdong; Bengtsson, Tord; Blennow, Jörgen; Gubanski, Stanislaw, *Arbitrary Waveform Impedance Spectroscopy used for Accurate Contact-free Dielectric Characterization,* 2012 International Conference on High Voltage Engineering and Application (ICHVE 2012), (Article no. 6357019) p. 170-173

3: Xu, Xiangdong; Bengtsson, Tord; Blennow, Jörgen; Gubanski, Stanislaw, *Enhanced Accuracy in Dielectric Response Material Characterization by Air Reference Method*, submitted for publication to IEEE Transactions on Dielectrics and Electrical Insulation

2 Background

In this chapter, the background of this thesis work as well as some literature studies is presented.

2.1 Dielectric response measurements

Dielectric response measurements are one of the two major non-destructive insulation test techniques in high voltage engineering. The other main technique is the detection and quantification of partial discharges. Dielectric response measurements are applied both in insulation material studies, to develop and characterize material for construction, and in apparatus diagnostics.

When a dielectric material is subjected to an electric field, the well-known effects of dielectric polarization and conduction are initiated [7, 8]. The dielectric response is the quantification of these effects. Their testing is usually performed by means of measurements of polarization and depolarization current (PDC), return voltage (RVM), insulation resistance (DC resistance) as well as variations of capacitance and loss factor in the frequency domain (FDS). Therefore, the dielectric response measurements can in general be divided into time domain and frequency domain categories. More information on conventional dielectric response techniques can be found in [9-13]. In this study, the focus is on improvements of measurement techniques for the frequency response characterizations, often known as frequency domain spectroscopy (FDS).

2.1.1 Interpretation of dielectric dynamic proprieties

Dynamic dielectric properties result from the presence of different polarization processes acting within a dielectric material under electric stress. These can either be described in time or frequency domains [8]. In the frequency domain, dynamic properties of dielectrics are expressed in terms of complex relative permittivity $\tilde{\varepsilon}_r(\omega)$:

$$\tilde{\varepsilon}_r(\omega) = \varepsilon_r'(\omega) - j[\varepsilon_r''(\omega) + \sigma_0/\varepsilon_0\omega] \tag{2.1}$$

where σ_0 represents the 'pure' DC conductivity of the material. If the applied voltage is maintained for some time, a polarization current can be measured. The amplitude of this current will change with time even if a constant voltage is applied. As in practical measurements of the dielectric response the contributions to the total current from the DC conductivity and the dielectric relaxation processes cannot be easy distinguished, the complex relative permittivity can further be denoted as:

$$\tilde{\varepsilon}_r(\omega) = \varepsilon_r'(\omega) - j\varepsilon_r''(\omega) \tag{2.2}$$

The real part of permittivity represents the capacitive contribution of a test object, whereas the imaginary part represents its losses. Both of them are dependent on frequency. Therefore, the recognized definition of complex capacitance $\tilde{C}(\omega)$ of a test object can be defined as:

$$\tilde{C}(\omega) = C_0\, \tilde{\varepsilon}_r(\omega) = C'(\omega) - jC''(\omega) \tag{2.3}$$

where the geometrical capacitance $C_0 = \varepsilon_0 A/d$ for a two parallel electrodes capacitor; A is the electrode area and d is the gap distance between two electrodes.

The loss factor $\tan \delta$ can further be denoted as:

$$\tan \delta = \frac{\varepsilon_r''(\omega)}{\varepsilon_r'(\omega)} = \frac{C''(\omega)}{C'(\omega)} \tag{2.4}$$

Dielectric response measurements in frequency domain can be very time consuming at low frequencies. More than one cycles of an AC voltage waveform are needed to determine amplitude and phase shift between the applied voltage and the response current. Therefore, several hours are required to perform frequency response measurement when frequencies lower than 0.001 Hz are aimed for. Since results of relaxation current measurements can be converted into the frequency domain and vice versa in case of linear dielectrics, both methods can complement each other. The measurement dielectric response at reasonably high frequencies (10 Hz to 10^6 Hz), may also require several minutes. Therefore, a testing voltage with rich harmonics content may be an attractive option as it allows determining the frequency response at harmonic frequencies with a single measurement.

2.1.2 Dielectric response instrumentation

Information on dielectric behavior of materials within a broad frequency range is important for new developments as well as for final quality control of electrical apparatuses. Primarily, too high losses at operation frequencies may cause thermal breakdown. Secondly, the quality and tolerance of electrical equipment can be estimated from dielectric measurements. Therefore, there is a considerable interest in such measurements.

Measurement techniques for dielectric properties in the frequency domain are very similar to the techniques used for measuring complex capacitances which has been under development for more than a century. These techniques can be roughly classified into three different generations which will be discussed below.

To measure the loss factor as well as the capacitance at power frequency, the standard measurement procedures are based on so called null methods [1], implying that a bridge circuit is balanced. Advantage of using bridge is that the dielectric properties can be measured as function of voltages. A famous and the most commonly used bridge is the high voltage Schering bridge, illustrated in figure 2.2. This bridge measures the capacitance and loss factor of a test object C_x by comparing it to a gas-filled standard capacitor C_N, which has negligible loss, both located at the high voltage arm. By adjusting variable resistors R_1 and capacitors C_1 at the low voltage arm, both sides of a null detector can be set to the same potential. The dissipation factor can then be calculated. Apart from the Schering Bridge, other bridges like transformer bridges, current comparator (Glynne) bridges and the parallel-T bridge use similar principles to determine loss factor as well as capacitance of an object. As each frequency needs to be carefully balanced, the whole measurement process is, however, very time consuming. Other drawbacks, like the requirement of expensive standard capacitors and sensitivity to harmonic disturbances are limiting the application of bridges.
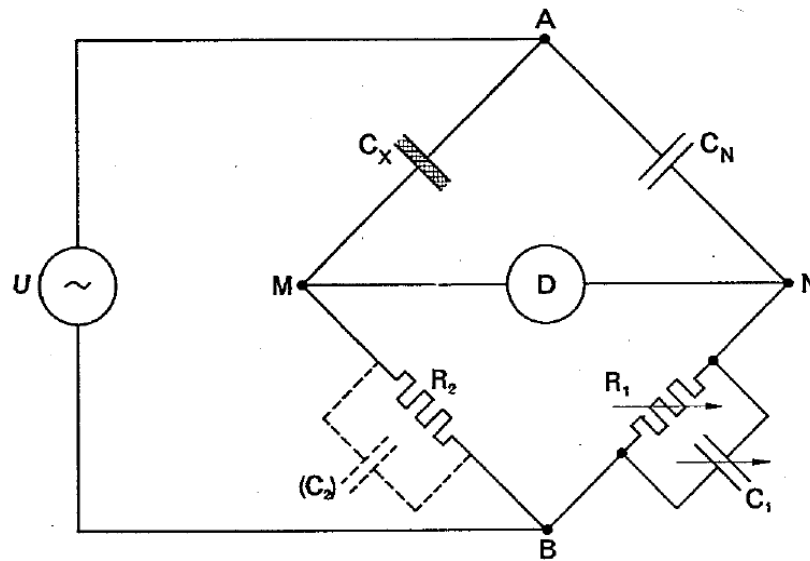
Figure 2.2: Circuit diagram of high voltage Schering bridge [1].

Due to the development of computational ability of modern computers, a digital Fourier transform could be performed decently fast with a thousand samples in the 90's. A new generation of dielectric frequency response measurements techniques was then made possible, where the voltage applied to a specimen and its response current waveform are digitized. The waveforms are transformed from the time domain to the frequency domain where the complex value of the frequency peak provides information on phase and amplitude at the dominating frequency. From the complex voltage and current values, the complex capacitance of test object can be calculated. However, mainly due to algorithm limitations, the test frequency and the digitizer need to be controlled simultaneously to sample full periods of the test signal, therefore measurements can only be performed with a well-controlled voltage source. Further, the resolution of the digitizer limits the measurement precision. More detailed descriptions and applications of this technique can be found in [10, 11, 14, 15].

In the present millennium, computers have allowed performing Fast Fourier Transform (FFT) of a million samples within seconds. At the same time, high-resolution digitizers also became available. With the addition of more computationally demanding signal analysis techniques [16-20], another generation of dielectric frequency response measurement techniques became possible. With these techniques, it is no longer necessary to adjust the digitizer to the test frequency. Therefore, in principle any type of voltage source can be used and harmonics can be applied as testing source for dielectric response analysis. This means that a full frequency spectrum analysis for dielectric response can be performed by a single measurement and on-line monitoring and diagnostic of electrical apparatuses becomes possible. Another example of such a technique is Arbitrary Waveform Impedance Spectroscopy (AWIS), which is described in [6, 21, 22]. Compared to other commercial instruments, for example IDAX [14, 23] and DIRANA [24], AWIS is more a concept than a defined instrument, which means that the user has to arrange a suitable voltage source and select appropriate and practical measurement provisions. Therefore,

this measurement technology is still developing and new applications are explored. In dielectric response measurements, limitations have become apparent in some applications. For example, too high harmonics content will cause aliasing effect; crosstalk between two signal channels; characterization of measurement circuit etc. The present thesis is based on this technique with the aim to further improve it and develop an accurate, fast way to characterize dielectric materials.

2.1.3 Electrode influence on losses

Apart from dielectric response signal acquisition and processing techniques, one of the most critical bottlenecks in dielectrics characterization is the electrode arrangement. When performing dielectric response measurement, the first question is how to apply a potential to the specimen. In general, a dielectric material should be placed between two electrodes to which the potential is applied. The size, shape and interface of these electrodes directly influence the current quantities measured, from which dielectric dynamic properties are derived.

The loss factors of modern insulation materials have a range from percent down to the 0.01% range. Many instruments are capable to determine such low losses. However, a low reproducibility and accuracy of the results becomes always a problem if the electrodes do not
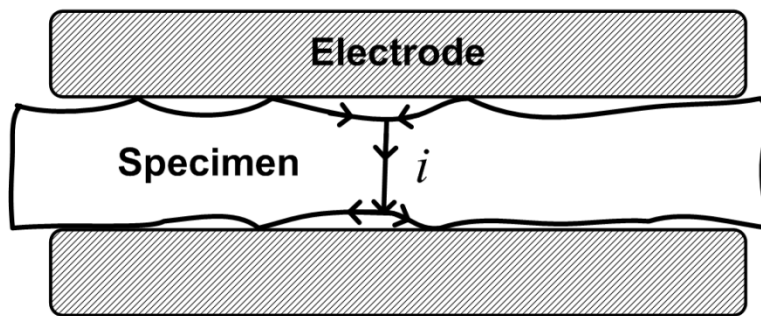

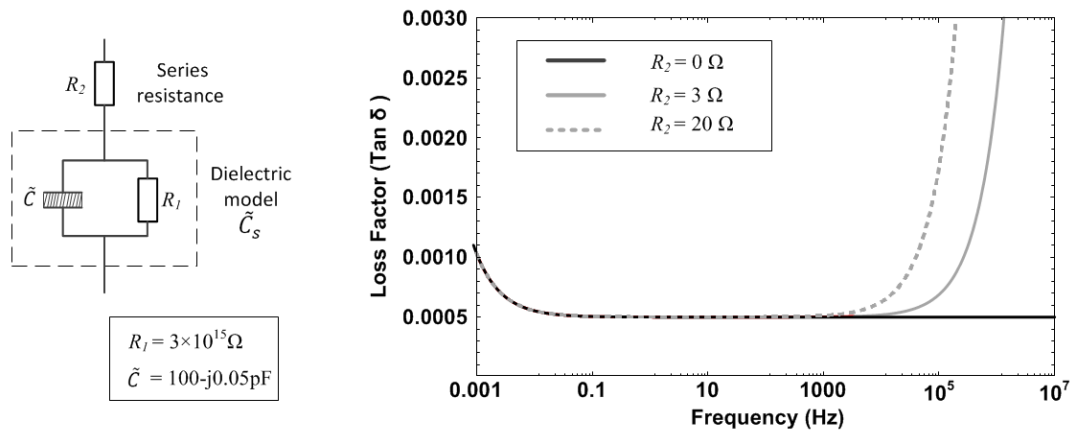Figure 2.3: Surface current paths due to insufficient contact between specimen and electrodes.

Figure 2.4: Model of dielectric with different series resistances and the resulting total losses.

6

make perfect contact over their entire area with the specimen. For example, an air gap of 0.01 mm in series with a specimen, having a relative permittivity of 3 and thickness 1 mm, will result in an error of 3% in the dielectric constant. The loss factor will also be influenced. Moreover, as shown in figure 2.3, an uneven surface contact will result in just a few contact points which add a series surface resistance. As shown in figure 2.4, a small series resistance added to a dielectric model, strongly increase the loss factor at higher frequencies. Equation 2.5 gives the total capacitance approximation of the model in figure 2.4 at high frequencies, where the C_s represents the dielectric specimen and R_2 is the series resistance attached to it. When the frequency increases, the losses due to R_2 will dominate and obscure the real losses. Further, equation 2.6 gives the total capacitance approximation of the model at low frequencies, where the parallel resistance R_1 will dominate and increase the losses. Here, R_1 represents the 'pure' DC conductivity of the material.

$$\tilde{C}_{tot} = \tilde{C}_s\left(\frac{1}{1+j\omega R_2\tilde{C}_s}\right) \approx \tilde{C}_s(1 - j\omega R_2\tilde{C}_s), \text{ when } f \rightarrow +\infty \tag{2.5}$$

$$\tilde{C}_{tot} \approx \tilde{C}\left(1 + \frac{\tilde{C}}{j\omega R_1}\right), \text{ when } f \rightarrow 0 \tag{2.6}$$

Thus, it is evident that proper surface contact between specimen and electrodes is one of the main requirements to obtain accuracy and reproducibility, particularly at higher frequencies.

The simplest electrodes would be two metal plates between which the specimen is placed. If the surface of specimen and electrodes were smooth enough, this would be acceptable. However, in most cases the specimen surfaces are not perfectly plane. Thus, surface contact problems often make this electrode arrangement practically useless. Many different types of electrode arrangements have been described and used for achieving a proper material surface contact [1, 2, 25], however, each of them has its advantages as well as its drawbacks. Among them depositions of conducting material on the specimen surface, such as fired-on metal films, silver painting or sputtering [26], conductive glue or grease with metal foil [25, 27], mercury and water solution of NaCl [1, 2] are popular solutions. An example is shown in figure 2.5, where a specimen is floating in a tray of mercury which serves as one electrode. A confining ring is placed on top of the specimen into which a pool of mercury is poured and serves as the other electrode. A "liquid" metal electrode may however change the dielectric properties and be toxic, for instance, fired-on metal and sputtering may heat up and change the surface properties of specimens, thin specimens may also absorb paint solvent, graphite applied from a suspension in a liquid may penetrate the specimen. With thin foil electrodes, it is difficult to determine the effective size of electrodes as well as the effective thickness of specimen as they are usually employed for non-uniform specimens. Comb electrodes mentioned in [28] may provide higher test capacitance and proper surface contact, but they are hard to fabricate and not easy to recycle. The electrode arrangements mentioned above share one common limitation: their preparation is time consuming. Some other electrode systems, such as semiconducting rubber electrodes [25] may be easy to use but may deform the specimen and will yield increased loss factors at high frequencies due to the electrode material resistance.
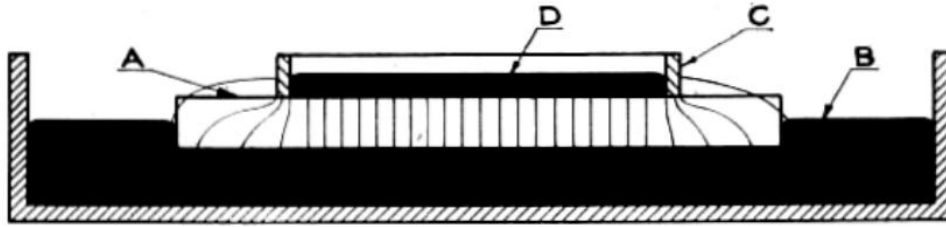
Figure 2.5: Mercury electrode arrangement suggested in [2].

A simple solution to the contact problem is to entirely avoid any direct contact between the material and the parallel plate electrodes, thus measuring the combined response of a small air gap and the specimen. Without any pressure applied on the tested object and by elimination of the surface conductivity, a contact-free electrode arrangement seems like the ideal solution for avoidance of the material contact problem in dielectric frequency response measurements. Such an electrode arrangement was first introduced by A. Campbell [29] in 1906. It consisted essentially of a parallel plate air capacitor, with the specimen of dielectric inserted in the air gap but not necessarily filling the gap completely and the capacitance between the plates was measured. The dielectric constant and loss factor can be calculated from measured capacitance and the known dimensions of the air capacitor and the specimen. The computations are not as simple as for the contact electrode arrangements as the result must be compensated for the presence of an air gap and a slight error in determining the thickness of the specimen or gap distance results a much larger error in the final results. Therefore, contact-free electrode arrangement has been largely forgotten in determination of dielectric properties. During the last century a few publications [1, 2] mentioned contact free solutions, but none of them seems to have been put into practice, probably due to the accuracy limitations. In recent years, only [30] presented some results for polymeric dielectrics by using Agilent 16451B electrodes system, in which the principle of the contact-fee electrode arrangement is utilized. No error analysis was however provided and the loss factor results were only provided at 50 Hz. In this thesis work, an air reference method as well as error analyses are discussed for contact-free measurements in detail.

2.1.4 Effect on permittivity measurement

When a high precision is required in permittivity measurements, the largest source of uncertainty comes from the dimensions of the specimen. The thickness accuracy depends on the surface roughness as well as the distance measurement accuracy. One reason is that rough surface will make loose surface contacts and creates several series resistances (both contact resistance and specimen surface resistance) as well as some air gap capacitances to the specimen. Another reason is that with rough surface or uneven specimen, the effective thickness of specimen is hard to determine with high precision. On the other hand, the specimen area should be large enough to provide a test object with high enough capacitance to enable measurements with the desired accuracy. Most existing instruments can measure capacitances in the range of 10 pF with 1% accuracy [1].

Another error source in permittivity measurements is coming from variations of electrostatic flux that bends and spreads out at the edge of electrodes, as illustrated in figure 2.6. The edge effect is
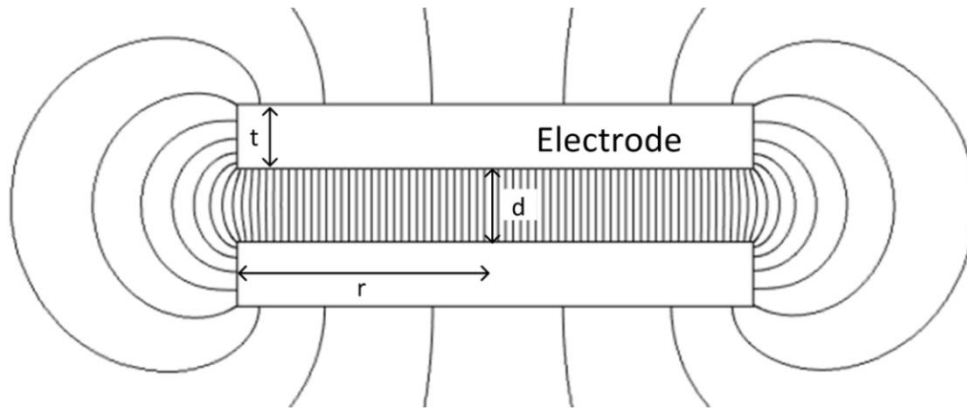
Figure 2.6: Electric field distributions between two parallel equal circular electrodes

also a known issue in capacitance measurements which researchers were struggling with for more than a century [2, 31, 32]. There are two common ways to limit this effect, one is to use a guard ring, which confines the effective specimen area [33], another one is to compensate the measured capacitance with a correction factor [34].

The classic way to compensate the edge effect from equal circular electrodes is to compare with the total capacitance computed from Kirchhoff formula [35]

$$C = \varepsilon_0 \frac{A}{d} + \varepsilon_0 r (log \frac{16\,\pi(d+t)r}{d^2} + \frac{t}{d} log \frac{d+t}{t} - 1) \tag{2.7}$$

where C is the total capacitance of two parallel circular electrodes with an air gap distance d and A is the electrode's surface area which is intended to be in contact with specimen; r and t are the radius and thickness of the circular electrodes.

For very thin electrodes, such as foil electrodes, the thickness of the electrodes t can be neglected. Thus the total capacitance reduces to

$$C = \varepsilon_0 \frac{A}{d} + \varepsilon_0 r (log \frac{16\,\pi r}{d} - 1) \tag{2.8}$$

One should notice that Kirchhoff formula is primarily applied to electrodes in air. To apply this formula correctly in dielectric material characterization would require that the electrodes be completely surrounded by a considerable volume of dielectric. Otherwise, as the electric field pass partly through air and partly through the specimen, the accuracy will degrade due to the difference in permittivity between the media. The detailed comparison of Kirchhoff's formula with other electrode arrangements, which preliminarily are designed to avoid edge and surrounding effect, can be found in [3].

Several scientific publications as well as standards [3, 32, 33, 36-38] present corrections to this edge effect with empirical equations or analytical expressions for various electrode configurations, such as unequal disk electrodes, electrodes with guard ring, thin film electrodes and so on. For instance, table 2.1 presents the IEC 60250 standard [1] recommended methods to calculate the capacitances of disk electrodes both with and without guard-ring. For the disk

electrodes with guard-ring, correction for edge capacitance is 0. The other disk electrodes that are without guard-ring employ a similar principle as the Kirchhoff formula and the corresponding correction factors for the edge effect are given.

The suggested corrections can improve the accuracy of permittivity measurements to some extent. The third inherent source of error from external objects, such as shield metal box and electrode supports, may however still degrade the measurement precision. As illustrated in figure 2.7, this is due to some electric field lines do not pass through the specimen and increase the total measured capacitances. The size of the capacitance change is then dependent on the position of surrounding objects. This type of error was mentioned in a few papers [2, 3], when it comes to practical experiential arrangements, this error source is, however, largely forgotten. Figure 2.8 is used in paper [3] to illustrate the coupling capacitances from the surrounding to the electrodes.

Table 2.1: Calculation of vacuum capacitance and edge corrections (From IEC 60250 standard)

(1)	Direct interelectrode capacitance (units: pF and cm) (2)	Correction for edge capacitance (units: pF and cm) (3)
1. Disk electrodes with guard-ring		
Eprouvette Specimen	$C_0 = \varepsilon_0 \cdot \dfrac{A}{h} = 0.088\ 54\ \dfrac{A}{h}$ $A = \dfrac{\pi}{4}(d_1 + g)^2$	$C_e = 0$
2. Disk electrodes without guard-ring		
a) Diameter of the electrodes = diameter of the specimen Eprouvette Specimen		When $a \ll h$ $\dfrac{C_e}{P} = 0.029 - 0.058 \log h$ $P = \pi d_1$
b) Equal electrodes smaller than the specimen Eprouvette Specimen	$C_0 = \varepsilon_0 \cdot \dfrac{\pi}{4} \cdot \dfrac{d_1^2}{h}$ $= 0.069\ 54\ \dfrac{d_1^2}{h}$	$\dfrac{C_e}{P} = 0.019\,\varepsilon_1 - 0.058 \log h + 0.010$ $P = \pi d_1$ Where: ε_1 is an approximate value of the specimen relative permittivity, and $a \ll h$
c) Unequal electrodes Eprouvette Specimen		$\dfrac{C_e}{P} = 0.041\,\varepsilon_1 - 0.077 \log h + 0.045$ $P = \pi d_1$ Where: ε_1 is an approximate value of the specimen relative permittivity, and $a \ll h$
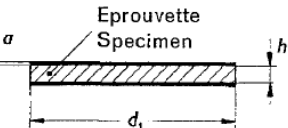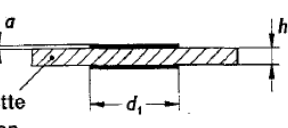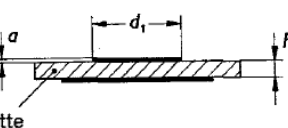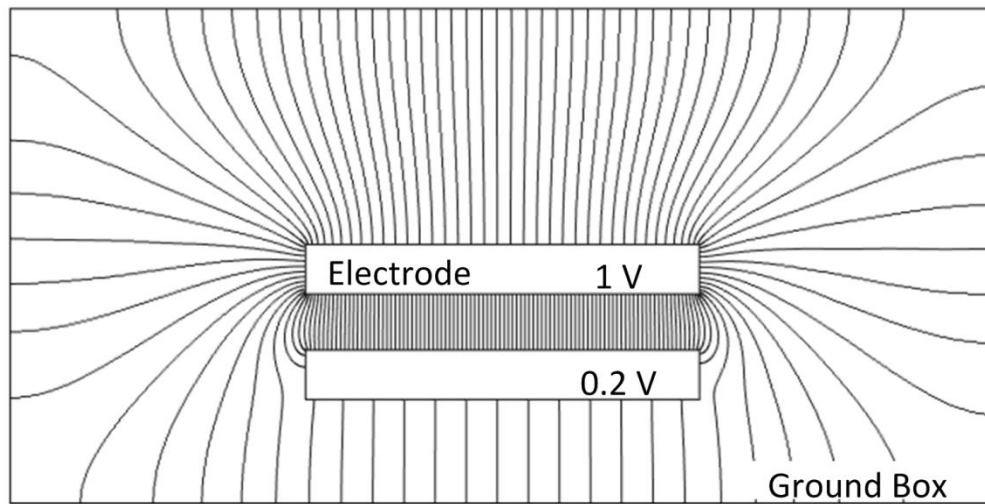
Figure 2.7: Electric field distributions of two parallel circular electrodes enclosed by a ground box; the electric potential of top electrode is 1 V and the bottom electrode is 0.2 V.
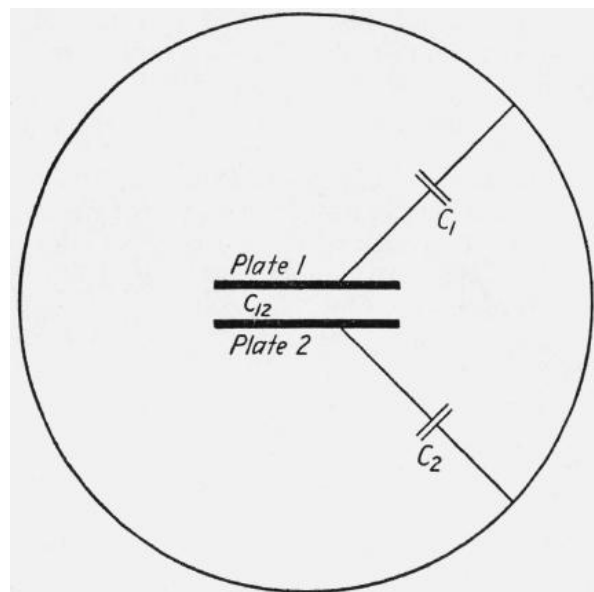
Figure 2.8: Diagram illustrating the coefficient of capacitance of two parallel plates with surroundings, copied from [3].

If the dielectric specimen is placed between plate 1 and plate 2 in Figure 2.8 and its permittivity is to be determined, C_{12} is the capacitance that needs to be measured, apart from the electrode edge effect. Assuming that the voltage potential is applied at the plate 1 and the current is measured from plate 2 (low voltage potential electrode), it is clear that the existence of C_2 will influence the measured capacitance and thus need to be eliminated.

Further, if a guard-ring electrode is used to confine the electric field lines and avoid the edge effect of electrodes, the capacitance between grounded guard-ring electrode and the low potential electrode will influence the accuracy as they are very close to each other. This is illustrated in figure 2.9 (a), and it is used to demonstrate the electrode arrangements in the measurements.

Interference from the surroundings can be largely avoided by some specially designed electrode arrangements, as for example the one shown in figure 2.9 (b). By using two identical dielectrics and placing them between three electrodes, the generated current is measured from the middle but smaller electrode, which is largely shielded by the other two electrodes to which the same voltage potential is applied. The drawback of this electrode arrangement is however that two identical specimens need to be employed.

In chapter 6, two possible solutions to reduce the geometric effect in accurate determination of dielectric constants are discussed. One is using a finite-element model of the electrode arrangement to estimate a needed correction. The acceptable degree of complexity in the model will however limit the degree of accuracy improvement. The other solution it to use a shielding guard electrode that covers the low voltage potential electrode entirely, except for the side where the specimen is attached. Furthermore, the voltage on the shielding guard electrode should preferably be the same as the low voltage electrode for avoid interference. The origin of this interference arises from the potential difference caused by the current measurement method. It especially needs attention in case of currents measured over a shunt and the measured capacitance is small. For other current measurement techniques, such as current transformer or current operational amplifier, this interference may not be so severe. In this work, we are however mainly focusing on current measurements by shunts, as this method allows for a wider flexibility in frequency and voltage characteristics.
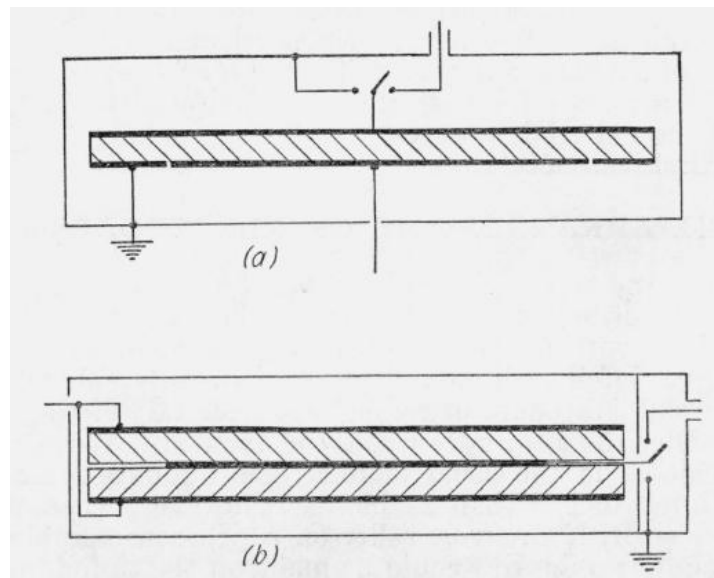

Figure 2.9: Two electrode arrangements to determine dielectric permittivity, suggested in paper [3].

2.2 Resume of previous work with AWIS

Power electronics are extensively used in utilities in the recent decade, which give rise to high harmonics content in the voltage waveforms in power system. The resulting electric stress on high voltage insulation materials is very different from before. Several failures [39, 40] have been reported due to high harmonic content which caused dielectric heating and fast rise times of the voltage can initiate partial discharges (PD). Therefore, the loss factor "tan δ" of dielectric material over a broad frequency spectrum attracts more and more interest.

With development of modern instrumentation technology and computational ability, AWIS has been developed for insulation dielectric diagnostics [4-6]. The main advantage of this technology compared to other conventional methods is that a well-controlled sinusoidal voltage waveform with precisely known frequency is no longer necessary to perform high precision dielectric response measurements. In traditional frequency domain (FDS) measurements, the voltage waveform is a concern as the acquisition system should be synchronized to the applied test frequency to sample full cycles of the waveform. The curve fitting implemented in AWIS makes synchronized sampling unnecessary. Further, harmonics in the applied voltage is not a problem for AWIS and, in principle, any type of signal can be used to perform measurements [6, 8, 22]. Another advantage for using AWIS in dielectric material characterization is that an entire dielectric spectrum can be determined from one single measurement with a test voltage source that contains high enough harmonics. Therefore, imprecise sources such as power voltages can be applied. The modest requirements on the test voltage signal make AWIS a good candidate for field on-line monitoring of dielectric properties in high voltage equipment.

In the development of the AWIS concept, a measurement toolbox based on this technique where gradually built. In order to meet the high demands on precision in dielectric response measurements, typically in the order of 10^{-4}, efforts were made to limit the stray capacitances and line inductances, at the same time, the inherent properties of the circuit components were considered. However, stray capacitance as well as line inductance cannot be completely eliminated. In order to cope with these, modeling of the measurement circuit over a broad frequency spectrum (from 100 Hz to 100 kHz) was carefully performed for both low and high voltage setups. For the high voltage setup (applied voltage is higher than the voltage specification in the DAQ card), a voltage divider were applied with consideration of its frequency responses.

The principle of dielectric response measurement employed in AWIS technique is a voltage-current measurement, a detailed description can be found in chapter 3. In high voltage applications, currents are normally measured through a current shunt, thus, shunt characterization becomes critical in a high precision measurement setup. In addition, measurements are performed over a broad frequency spectrum where the impedance variation of the measured "capacitor" is significant. Thus, in order to utilize the resolution of DAQ card optimally, the current shunt should preferably be capacitive. Therefore, in the AWIS measurement setup, the shunt was modeled as a resistance in parallel with a capacitance and a line inductance is included.

Further, the realized AWIS setup was used in several applications: The dependence of capacitance and loss on voltage, temperature and time where studied and significant effects were found. This resulted in a general formulation of how to calculate dielectric heating under voltages with a high harmonic content [21]. Further, the PD behavior of different objects was studied by monitoring the discharge current in both frequency and time domain. For example, the change of

dielectric properties during electrical tree growth in LDPE samples was studied by monitoring capacitances which usually were less than 1 pF [41, 42].

3 Experimental Setup

In this chapter, an experimental setup based on AWIS technique is discussed. This measurement system cannot only measure a dielectric response under voltages with a specified frequency but is also capable to determine an entire dielectric spectrum from one measurement, provided the test voltage is rich enough in harmonics. The precision of measurements is typically in the order of 10^{-4}. Such a precision requires all the circuit component properties to be considered and being well defined, such as shunt properties, crosstalk, stray capacitances and inductance of wiring. In order to limit the external interferences, the test object as well as the shunt and all the connections should be properly shielded and noise level in the order of 10^{-6} achieved.

3.1 Basics

The principle of dielectric response measurements is based on a voltage-current measurement, from which the complex impedance frequency response of the test object is obtained. The basic circuit for dielectric response measurements is shown in Figure 3.1.

By applying a voltage with certain frequency content $V_0(\omega)$ and measuring the voltage waveform of $V_0(\omega)$ and $V_1(\omega)$, the complex impedance of the test object $Z_{to}(\omega)$ is calculated through equation. 3.1.

$$Z_{to} = Z_{sh} \frac{V_0 - V_1}{V_1} \tag{3.1}$$

The Fourier transform technique employed by AWIS enables separation of harmonics if the applied voltage contains more than one frequency. Theoretically, any kind of repetitive voltage signal can be applied to obtain the dielectric frequency response of a test object, which makes on-line monitoring possible but the voltage waveform determines the harmonic content and thus defines the dielectric response spectrum, for example, an ideal square wave voltage contains all
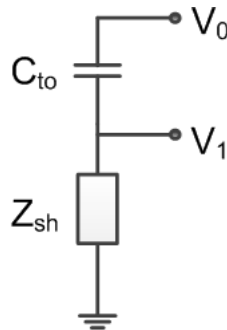

Figure 3.1: Principal circuit for dielectric response measurement of a test object (C_{to}). The shunt impedance (Z_{sh}) is used to measure the current passing through the test object.

the odd harmonic frequencies. In principle, the measured complex impedance of test object $Z_{to}(\omega)$ can contain all frequencies represented in the harmonic spectrum. However, the useful number of harmonics is limited by the signal to noise level as well as other interferences from the measurement circuit. Measures for avoiding the interferences such as matching of shunt impedance, crosstalk deduction and shielding are discussed in following.

3.2 Capacitive shunt

In order to perform a broad harmonic frequencies response measurement in the test set-up and make the best use of resolution of the data acquisition (DAQ) card, the amplitude of each measured signal should be as close as possible to the specified maximum voltage level of the DAQ card. Further, as the input range selected on the DAQ card has an influence on the frequency response, both channels should use the same range. In general, the harmonic amplitude will decrease with increasing harmonic number, n, as exemplified in Figure 3.2. For a square-wave, the harmonic components have 1/n dependence. Therefore, a capacitive shunt is favorable as the impedance of the test object can be matched with the shunt impedance over the desired frequency spectrum thus enhancing the signal strength at higher frequencies. Using an ideal capacitor as shunt is, however, not practical and the current shunt (Z_{sh}) need to be built by a capacitor in parallel with a resistor. The purpose of the parallel resistor is to stabilize the shunt capacitor by a controlled leakage current and avoiding floating potential. Without the resistor, the leakage current would be determined solely by stray conductance in the set-up which would introduce additional uncertainties. For low voltage tests (~10 V), the size of the shunt capacitance should be about the same order of the test object and the choice of shunt resistance determines the RC time constant, which is of importance when short pulses, such as partial discharges, are studied as presented in [43].

$$\tau = RC \hspace{4cm} (3.1)$$

The shunt resistor needs to be large enough to match the impedance of the test object at the lowest frequencies but also need to be small enough to stabilize the shunt capacitor. Figure 3.2 additionally shows two response voltages over different shunts. With a smaller shunt resistance, the response voltage amplitude over the measured frequency show less variation. A significant amplitude difference between the applied and measured voltages will, however, cause a substantial interference due to crosstalk. This is further discussed in section 3.3. Therefore, a relatively large shunt resistor (900 kΩ) is chosen to stabilize the shunt capacitor (330 pF). In addition, a voltage divider is employed to match the impedance of the test object and reduce crosstalk.

If the measurement is performed by sweeping a frequency with constant voltage amplitude, the response voltage amplitude is only determined by the impedances of the test object as well as the shunt.

Figure 3.3 illustrates an applied constant voltage and corresponding response voltages over three different shunts. The amplitude at low frequencies is defined by the shunt resistor and the level at high frequencies is controlled by the shunt capacitor.

A proper capacitive shunt should be suitable both for swept and harmonics measurements. As a result, change of current sensitivity at different frequencies is not needed in the setup, this

substantially reduces the work of measurement circuit characterization. Another advantage of applying capacitive shunt is that elaborate reduction of stray capacitance and line inductance from circuit components is no longer necessary as the influences from those components are included in the circuit characterization.

In an actual measurement set-up, a shunt must be calibrated for two reasons. One is that all electrical components have a limited accuracy and may have losses. Component losses may dominate the total losses if specimen losses are in the 10^{-4} range and modern insulation materials
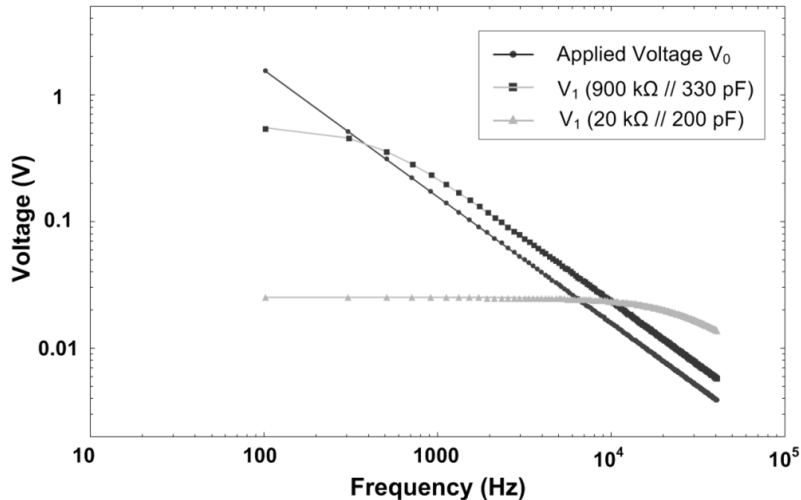
Figure 3.2 Applied voltage V_0 (a square shape like voltage waveform contents 200 odd harmonics, it is measured through a 6.4:1 voltage divider) and response voltage V1 measured over two different shunts (900 kΩ // 330 pF and 20 kΩ // 200 pF), the test object has capacitance $C_{to} = 100$ pF.
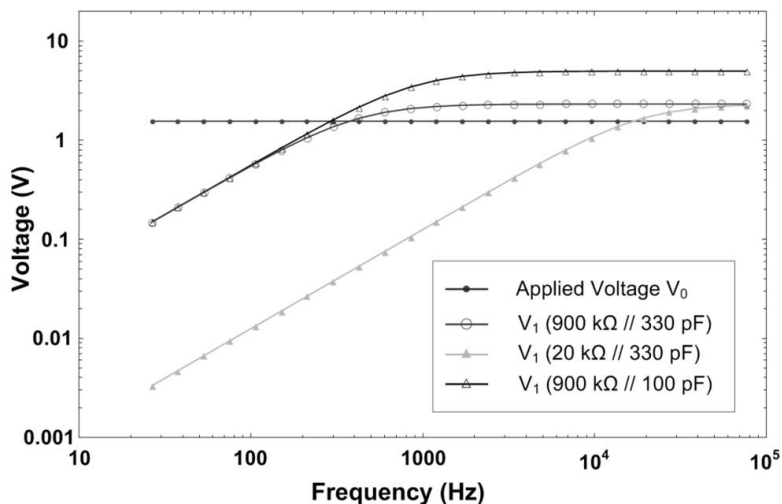
Figure 3.3 Swept voltages V_0 (a 10 V sinusoidal waveform measured through a 6.4:1 voltage divider) and response voltages V_1 over three different shunts (900 kΩ // 330 pF, 20 kΩ // 330 pF and 900 kΩ // 100 pF), test object capacitance $C_{to} = 100$ pF.

are often at this level. The other reason is that, in any electrical test set-up, stray capacitances and line inductances always appear and are very difficult to estimate. Stray capacitance and line inductance will always have some influence on the shunt properties.

To characterize a shunt with high precision, complicated circuit models are often required, which include the effects of the skin effect, temperature dependence and other small corrections need to be accounted for. Thus, there is a limit to how well a physical shunt could be modeled. As a capacitive shunt eliminates the need to change current sensitivity, relative calibration of the whole test set-up can be done by measuring an air capacitor under the same test conditions as specimen measurements, instead for an elaborate shunt characterization. This relative calibration can significantly increase the accuracy as influences from changing test environment are taken care of by "real-time" calibration, see section 5.

Active operational amplifiers (op-amp's) are presently widely used for current measurements as these provide much lower input impedance and thus reduce the voltage drop over a high impedance shunt. However, the main drawback of operational amplifiers in dielectric frequency response characterization is that all amplifiers have finite bandwidth. To a first order approximation, the gain of a typical op-amp is inversely proportional to frequency and is characterized by its gain-bandwidth product. Associated with the bandwidth limitation is a phase difference between input signal and the amplifier output that can even lead to oscillation in the amplifier. To avoid oscillation in the amplifier and to stabilize the feedback circuit, frequency compensation might be necessary and this reduces the bandwidth of the op-amp even further. Therefore, sensitive loss measurements become increasingly difficult at high frequencies with amplifier solutions due to the circuit time delay. Further, the temperature dependence of the electrical circuit, noises and the need to accurately characterize the measurement circuit are not eliminated by this technique.

3.3 Interference reduction

Interferences may exist in any electrical circuit due to electromagnetic coupling or radiation, which both may come from external sources and electrical components in the circuit itself. In the measurement system, interference or disturbance may interrupt, obstruct or otherwise degrade the measured signal and reduce the signal to noise level (S/N). In AWIS harmonic measurements, the high demand on measurement accuracy (in the order of 10^{-4}) and the decline of harmonic amplitude requires proper consideration of background noise level in the test setup. Therefore, reducing the crosstalk between two adjacent voltage channels and minimization of external noise are essential to satisfy the demands.

3.3.1 Crosstalk

Crosstalk in electrical measurement is the phenomenon by which a signal in one measurement channel creates an undesired effect in another channel. Crosstalk is usually caused by capacitive or inductive coupling from one channel to another. A more detailed description of crosstalk can be found in [4], where it is concluded that measurements on high impedances are especially vulnerable. High impedance components are often found in the AWIS measurement setup, for example, a capacitive shunt, therefore the two voltage channels are interfering with each other by capacitive crosstalk. Figure 3.4 shows a 7 V and 80 Hz sinusoidal signal that is measured by Ch0 and its corresponding crosstalk in an adjacent channel, Ch1 of a multiplexing DAQ card, which is
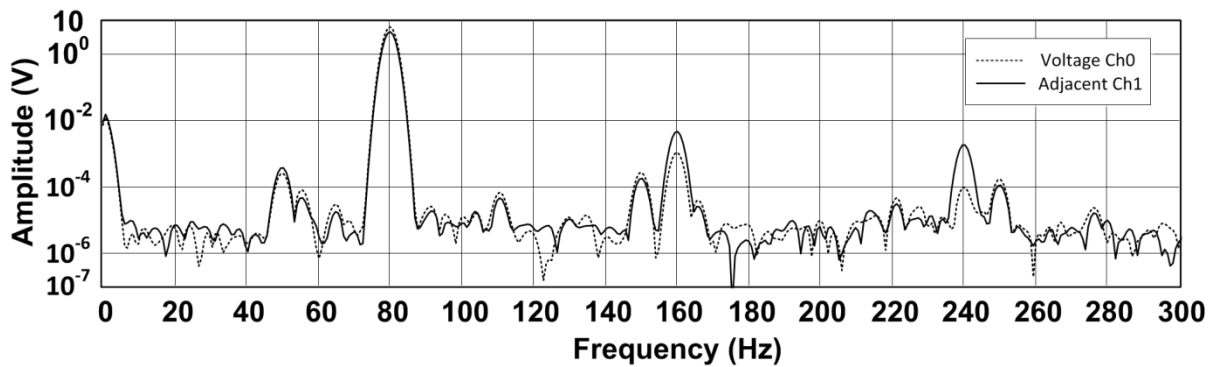
Figure 3.4: Applied voltage on Ch0 only (7 V and 80 Hz sinusoidal) and the corresponding crosstalk in the adjacent Ch1 which is connected through a capacitive shunt (a 330 pF capacitor in parallel with a 900 kΩ resistor) to ground. The sampling rate of DAQ card is set to 200 kS/s.

connect to the ground through a capacitive shunt. The amplitude of the two signals is almost identical, especially at fundamental frequency. The main reason for this result is that the multiplexing DAQ card has been used and, with high source impedance, the charge accumulated does not decay fast enough. To reduce crosstalk in the measurement setup, several methods are employed, which are discussed in following.

3.3.1.1 Operational amplifier

As one of the causes for crosstalk is due to high impedance of the test circuit, reducing the source impedance to the DAQ card is an effective way to reduce the crosstalk. However, a too small shunt impedance will reduce the S/N ratio and thus decrease the accuracy. An alternative way to reduce the input impedance of the DAQ card is to employ an operational amplifier [4] before the response voltage channel. In this setup, an OP42GP amplifier [44] with 1:1 amplification has been used and Figure 3.5 shows that application of the amplifier allows to reduce the crosstalk more than 100 times. All amplifiers have however a frequency dependent voltage response. This can either be handled by complex polynomial curve fitting [4] or it can be taken into account as a part of the shunt characteristics and normalized by the whole measurement circuit calibration. The bandwidth of the used amplifier is 10 MHz, which is much larger than the sampling rate of the DAQ card.

3.3.1.2 Multiplexing sampling

Another reason for crosstalk is due to the analogue input architecture of the DAQ card. The most commonly used architectures involve multiplexing or simultaneous sampling [45]. A comparison of the two architectures can be found in [4], where it is concluded that both of them have some disadvantages. For simultaneous sampling, each channel has its own amplifier, thus the response varies with channel. A multiplexing card uses the same amplifier but may suffer from crosstalk if the amplifier does not stabilize fast enough. The used DAQ card in the AWIS measurement setup is a multiplexing card. A simple method to avoid crosstalk between two adjacent channels is to separate them and discharge the amplifier by reading a grounded channel in between. The drawback is that the maximum sampling rate is reduced by half. Figure 3.6 illustrates the voltage levels in different channels by employing the grounded channels. The response voltage channel,
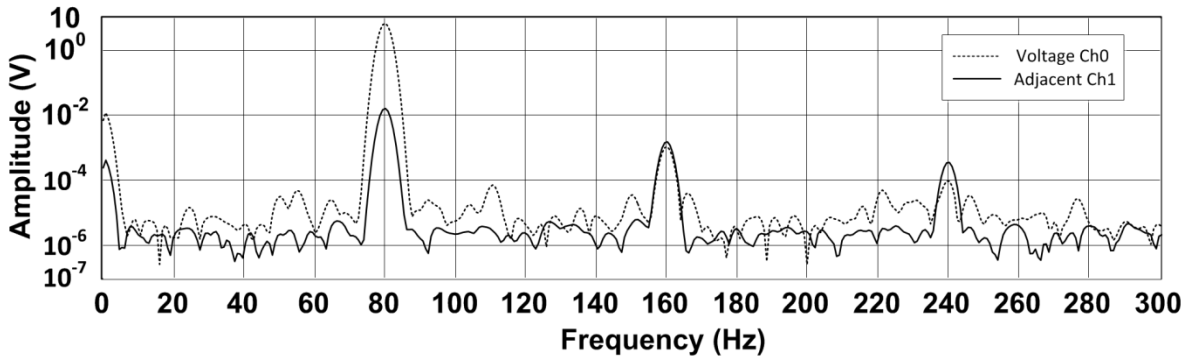
Figure 3.5: Applied voltage on Ch0 only (7 V and 80 Hz sinusoidal) and the corresponding crosstalk in an adjacent Ch1, which is connected through a voltage follower and in series with a capacitive shunt (a 330 pF capacitor in parallel with a 900 kΩ resistor) to ground. The sampling rate of DAQ card is set to 200 kS/s.
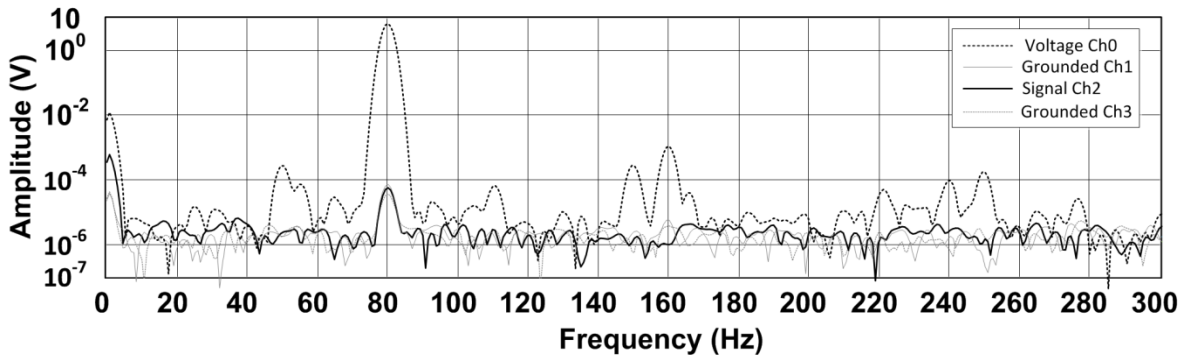
Figure 3.6: Applied voltage on Ch0 only (7 V and 80 Hz sinusoidal) and the corresponding crosstalk in an adjacent Ch2, which is connected through a 1:1 amplifier in series with a capacitive shunt impedance (a 330 pF capacitor in parallel with a 900 kΩ resistor) to ground, Ch0 and Ch2 are separated by another two short-circuited and grounded channels (Ch1 and Ch3). The sampling rate and voltage range of each channel is set to 200 kS/s and 10 V. For each signal, 270 kS are recorded and analyzed.

Ch2, is now at about the same level as the background noise and crosstalk is largely avoided by sacrificing the sampling rate.

3.3.1.3 Voltage divider

In AWIS measurements, the two measured voltage signals should preferably be at the same order of amplitude to maximize the accuracy of the DAQ card. It is therefore favorable to use a voltage divider to adjust that applied voltage signal to roughly the same amplitude as the response voltage signal. In the present low voltage measurement setup, two in series connected resistors are used as a voltage divider. Figures 3.7 and 3.8 show normalization of the frequency response of the voltage divider by a complex polynomial curve fitting. For high voltage measurements, a capacitive voltage divider may be favorable to limit the current through the divider. A purely resistive or capacitive voltage divider does not exist, however. There is always some frequency

dependence due to cabling and stray capacitances, as exemplified in the figures. For a capacitive divider it is usually beneficial to have a resistor in parallel to the lower capacitor, for similar reasons as in the shunt design.

Figure 3.7: The measured and curve fitted absolute value of the voltage division.
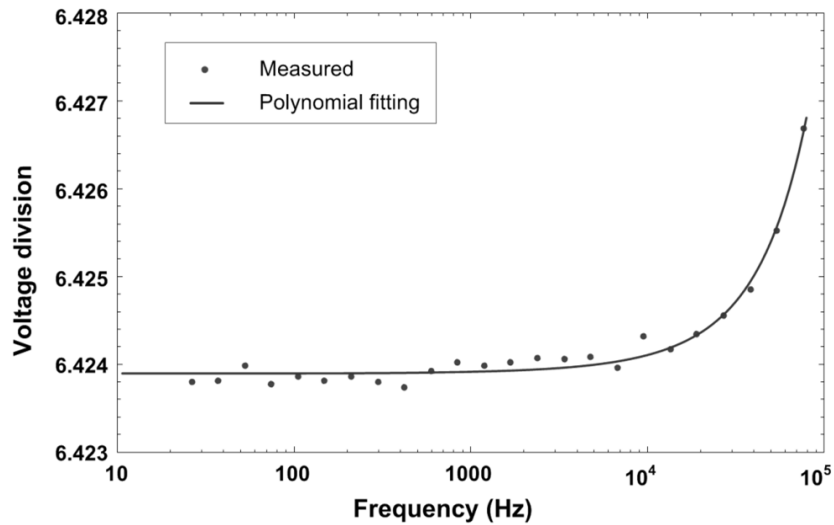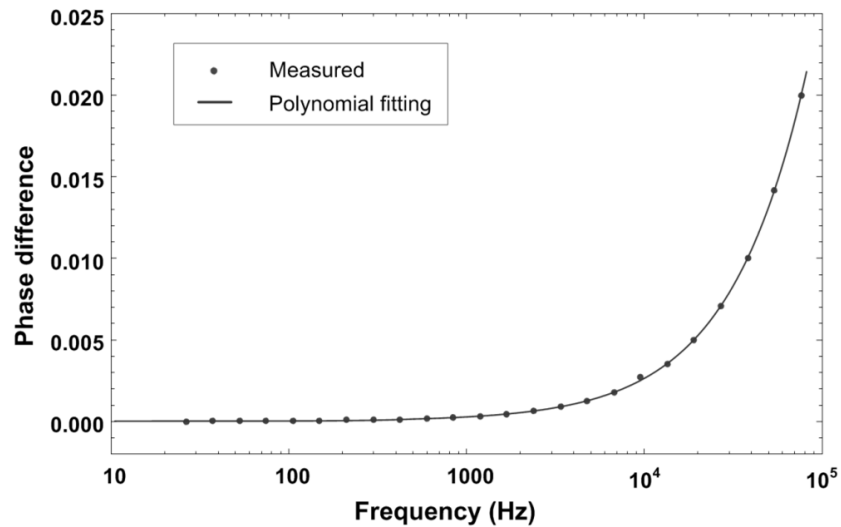

Figure 3.8: The phase difference between V_{in} and V_{out} of the voltage divider.

3.3.2 Noise

In an electrical system, noise is a random fluctuation and yet an unavoidable property of all electric circuits, often originating from temperature variations. In measurement systems, noise is an error or undesired random disturbance of a measured signal, introduced before or within the DAQ card. The noise level determines the useful signal amplitude (signal-to-noise ratio), therefore it is very important in the AWIS measurements especially when harmonics are to be utilized. The amplitude of harmonics decreases sharply with increased harmonic number. Figure 3.9 show the amplitude of the first 200 odd harmonics of a square-wave signal. The applied fundamental voltage is 1 V, resulting in 0.005 V at the last harmonic frequency. As modern dielectric materials have their loss factor in 10^{-4} range, therefore the background noise level determines how many harmonics that have a sufficient signal to noise ratio can be used in AWIS measurements and this limits the usable frequency spectrum.

A part of the AWIS technique is to utilize reduction of random noise by averaging. The noise from the average of N measurements is reduced by $\sqrt{N}$ as compared to the individual measurements. This is achieved by Fourier analysis of very long records, as long as it is practically possible for the measurement computer to handle. In this work, typically records with 270 kS are used. The value of this averaging effect is apparent from figure 3.9 by considering that a 16-bit DAQ card is employed which gives a digitalization noise higher than 5×10^{-5}, thus the averaging improves the signal to noise ratio about two orders of magnitude.

3.3.2.1 Shielding

Apart from noise generated by the measurement setup, noise from any external sources should be avoided at all reasonable costs. In general, use of a faraday cage is a good approach to block out most electromagnetic and electrostatic noise from a complete circuit. Putting a whole measurement setup, including DAQ card, voltage source as well as computer into one enclosure is, however, not practical. Therefore, in practice, only the electrode system is usually shielded with a grounded metal box but the whole circuit is connected through BNC cables, which can be considered as small faraday cages.
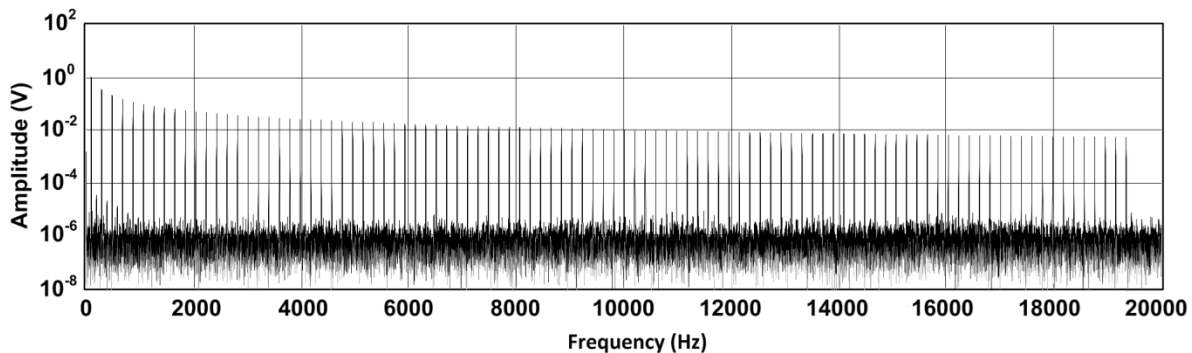

Figure 3.9: The measured voltage signal with a square like waveform which contains only 200 odd harmonics. The applied fundamental voltage is 1 V and 97.2 Hz. The sampling rate and measurement range are set to 200 kS/s and 2 V, and for each signal 270 kS are recorded for analysis.

3.3.2.2 Grounding

Proper common ground is essential in all sensitive measurements to reduce unexpected ground loops. Ground loops occur when there is a voltage difference between two grounding points and increase the noise level. Since ground is thought of as at 0 V, the presence of different potentials is undesirable at any point of a ground wire. If this is the case, it would not be a true ground. A good way to avoid this is to bring all the ground wires to the same ground point.

3.3.2.3 Voltage supply of amplifier

As a simple DC voltage supply of the amplifier can be one of the main contributors to the noise level, a very stable voltage source is desired. The power consumption of the OP42GP operational amplifier is very small, about 6 mW, at a high speed working mode. Thus, instead for an expensive stable laboratory power supply, which might anyhow contribute to the noise floor, use of alkaline batteries is a good alternative. Practical experience show that two 9 V alkaline batteries can supply the amplifier for more than a week.

3.3.2.4 Harmonics

Unexpected harmonics generated by voltage sources, amplifiers or any other test setup components will also increase the background noise level and decrease the accuracy. Therefore, it is necessary to evaluate the harmonic noise from the test setup. In Figure 3.10, a 7 V, 100 Hz sinusoidal voltage signal generated by a HP 33120A function generator was measured by the Ch0 of the DAQ card. In order to measure the noise from the amplifier, Ch2 was connected through the amplifier and in series with the capacitive shunt to the ground. Two additional channels, Ch1 and Ch3, were grounded and employed to separate the signal channels. Significant peaks are found at the even harmonic frequencies, 200 Hz and 400 Hz, about two decades above the noise level, and the voltage level at odd harmonic frequencies, 300 Hz and 500 Hz is also noticeable. As these noises are only found in Ch0 implies that these harmonics are present in the applied voltage waveform and are generated by the function generator. High noise at other frequencies are also apparent, for example, at 50 Hz and 55 Hz and their corresponding 2nd, 3rd and 4th harmonic frequencies, the amplitudes are one or two decades over the background noise level. The signal observed by Ch2 indicates that there is small crosstalk interference from Ch0 at fundamental frequency and it is about of the same amplitude as in the grounded Ch3. The noise level at 55 Hz of Ch2 is also visible, which indicates that noise at 55 Hz and its corresponding harmonic components at Ch0 do not come from the voltage source. Compared to the grounded channels, the signal from Ch2 shows that there is no significant harmonic components which might be generated by the amplifier. In addition, all measured signals show a substantial peak at 0 Hz, which indicates that the DC offset from the power supply or DAQ card is substantial.

It can therefore be concluded that disturbances from the harmonics and spurious distortion of the measurement setup can derogate the accuracy far more than the background noise. Though distortion of the voltage source is not harmful, as its inherent harmonics can either be filtered out or separated and used as the testing source by the AWIS technique, the power frequency (50 Hz) and the 55 Hz as well as their harmonic frequencies should be avoided. Even though the level of these are low (10^{-5} V), they will still affect the result if a low loss material (10^{-4}) is measured.

3.3.2.5 Results

The crosstalk and other noise were largely reduced by implementing the methods mentioned above. Figure 3.11 shows a measured frequency spectrum, where a 1 V, 8 kHz sinusoidal voltage and its corresponding response signal over an air gap capacitor are measured by Ch0 and Ch2 respectively and two grounded channels Ch1 and Ch3 are used to reduce the crosstalk. The figure indicates that the background noise level of the DAQ card is lower than 10^{-6} and the noise level of the test setup is close to 10^{-6}. Therefore, dielectric response measurement of a loss factor of 10^{-4} is possible for the 100th harmonic if the applied voltage signal is in the range of 1 V.
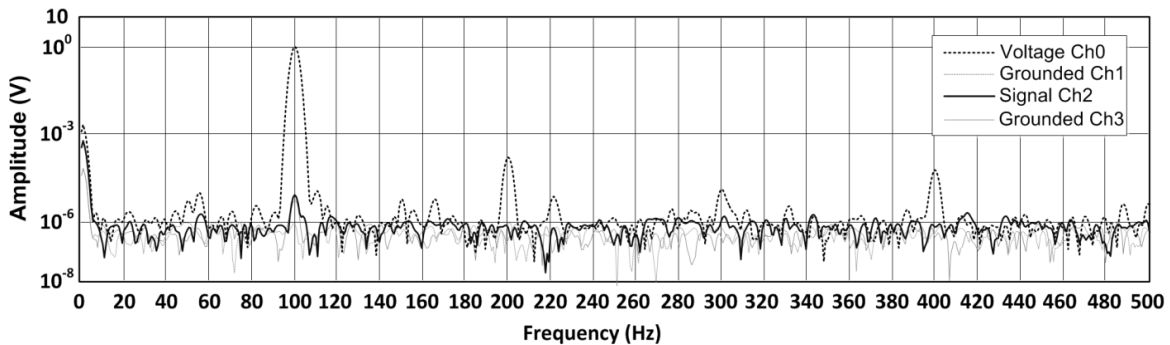
Figure 3.10: Noise levels of the DAQ card at low frequency, Ch0 is measuring a 7 V, 100 Hz sinusoidal voltage through a voltage divider, Ch1 and Ch3 are directly grounded and Ch2 is connected through an amplifier and a capacitive shunt to ground.
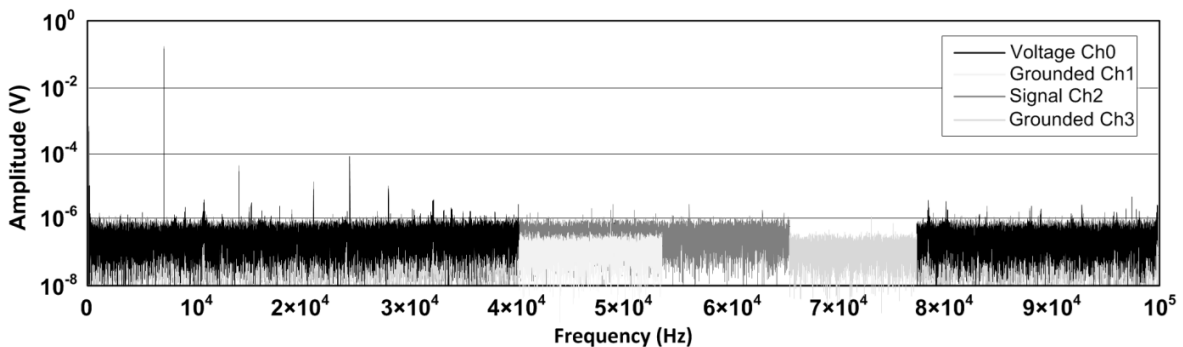
Figure 3.11: Noise levels of the whole frequency spectrum; a 1 V, 8 kHz sinusoidal voltage is measured through the voltage divider by Ch1 and its response signal over an air gap capacitor is measured by Ch2; responses of two grounded channels Ch1 and Ch2 are also shown. The sampling rate and measurement range of each channel is set to 200 kS/s and 1 V. For each signal, 270 kS are acquired and analyzed. In order to show the noise level of all signals, several parts are removed from the figure.

3.4 Final test setup

The implemented AWIS final test setup is illustrated in figure 3.12. In order to generate the voltage signal for dielectric response studies, a 15 MHz arbitrary waveform generator (HP 33120A) [46] has been used as the voltage source in low voltage AWIS measurements. It has capability to generate a 12-bit 40 MS/s arbitrary waveform with the length ranging from 8 to 16,000 data points. In addition, other ten standard waveforms, such as sine, square, triangle, can also be generated. For sine waveforms, it has a non-harmonic spurious distortion less than -65 dB. The responding current over the test object (C_{to}) is quantified by the generated voltage over the capacitive shunt (Z_{sh}). To reduce the measurement noise, all the other circuit components are shielded in a shielding box apart from the voltage source (Function generator) and DAQ card. The used DAQ card is a 16-Bit, 1.25 MS/s multiplexing card (NI USB-6251). To avoid crosstalk interferences in the multiplexing DAQ card, a voltage divider and an amplifier (OP42GP) is installed in the applied voltage channel (Ch0) and in the responding current channel (Ch2) respectively. Further, two grounded channels (Ch1 and Ch3) are used to separate the two signal channels.

Figure 3.12: Schematic diagram of the experimental setup.

4 Harmonics Limited Waveform

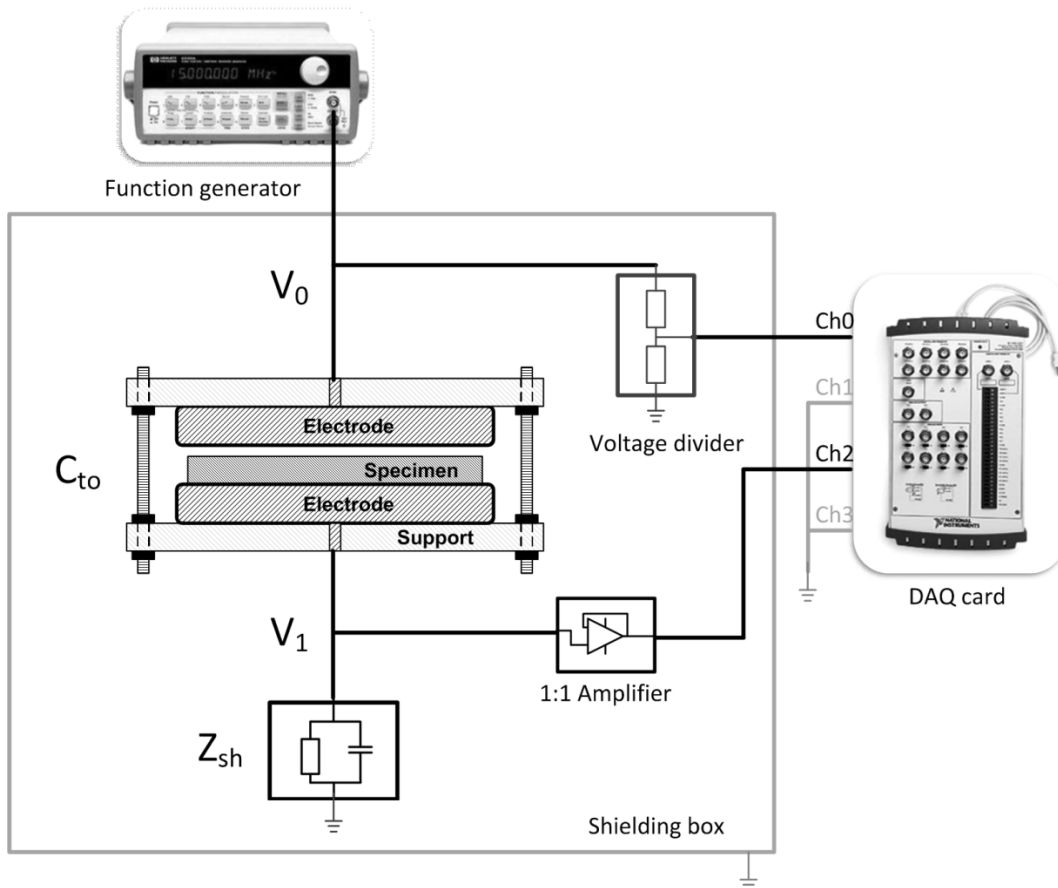AWIS is capable of determining an entire dielectric spectrum from one measurement, provided the test voltage is rich enough in harmonics. However, extremely harmonic-rich test signals limit the measurement accuracy due to aliasing. In this chapter, a practical method to eliminate the aliasing from the measurements is discussed.

4.1 Aliasing

Aliasing is caused by the data acquisition by the harmonic frequencies above the Nyquist frequency (half of the sampling frequency). However, anti-alias filters, the customary solution, are preferably avoided when using AWIS due to high precision and sensitivity requirements. An alternative solution is to control the aliasing by limiting the test signal harmonic content. In this chapter, optimized waveforms, which can be applied in situations where the test voltage is not dictated by other requirements, are presented. In such cases, it enables the use of AWIS for fast dielectric studies under rapidly changing environmental conditions. A complication with generating optimized test waveforms is that "harmonic groups" aliasing appears. A practical method to control the "harmonic groups" is therefore discussed.

It was shown in [6] that due to the aliasing in the signal sampling process, the harmonics with frequency above the Nyquist frequency fold back and severely affect the measurement accuracy.

Figure 4.1 illustrates how a sinusoidal single waveform (grey curve) is sampled at a periodic interval (dots), and the black curve with lower frequency is the perceived result. If the number of harmonic content continues and is high enough, the perceived aliasing frequencies, f_a, will show a fold back behavior [4, 47]. In AWIS measurements, it may happen that a harmonic component below $f_s/2$ is polluted by an aliased component and the result will be a mixture of the response at the involved original frequencies.
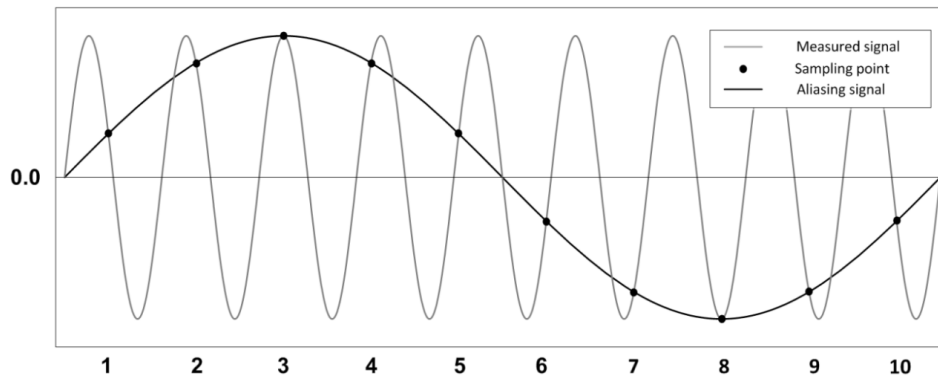
Figure 4.1: Example of aliasing in periodic sampling, a sinusoidal signal $f = 0.9$ sampled with $f_s = 1$ and its corresponding aliasing signal with $f_a = 0.1$.
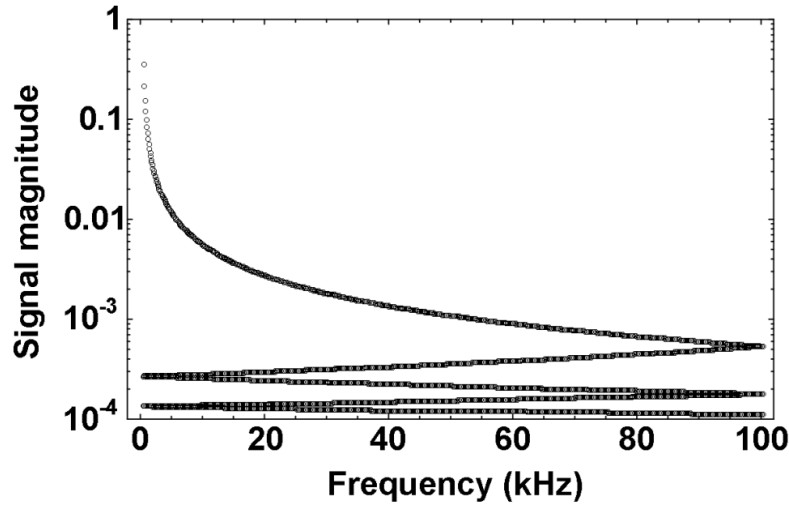
Figure 4.2: Folded harmonics of a square voltage waveform with fundamental frequency 42 Hz and a sampling rate of 200 kS/s. As the square wave has linearly decreasing harmonic amplitudes, the original frequency is here reflected in the signal magnitude.

The folding behavior is shown in Figure 4.2 and it can be described by equations 4.1 or 4.2 [4]. Equation 4.1 is used when $2f/f_s$ is even and equation 4.2 if $2f/f_s$ is odd.

$$f_a = f \bmod (f_s / 2) \tag{4.1}$$

$$f_a = (f_s - f) \bmod (f_s / 2) \tag{4.2}$$

4.2 Test waveform

Anti-alias filters, which are the customary solution, are not particularly effective due to the high precision requirements of AWIS. Such filters would namely have to be of very high order and identical to ppm precision for all used channels.

One solution to avoid the aliasing affect in dielectric harmonic measurements was employed in [4] by adjusting the sampling rate and the fundamental frequency to control the frequencies of aliased signals f_a. The minimum frequency separation (f_{ms}) is calculated, which is defined as the minimum distance between two perceived, aliased or true, frequencies. As large f_{ms} as possible is desired for reducing the possibility of overlapping the aliased signals with the harmonics, which are originally below the Nyquist frequency.

Another solution to improve the accuracy of AWIS measurement is to eliminate aliasing affect by limiting the harmonic content of the test waveform. In principle, the system response under a harmonics limited waveform is the same as under a square-wave waveform with an infinite order anti-alias filter. The harmonics limited waveform can be described by equation 4.3:

$$x_{limited}(t) = A \sum_{k=1}^{n} \frac{\sin(2\pi k f_f t + \varphi_k)}{k} \tag{4.3}$$

Figure 4.3: Example of two harmonics limited waveforms, both containing 100 odd harmonics and 2000 samples per period. The black waveform has all phases shifts equal to zero and the gray one has randomly distributed phase shifts.

where, n is the number of desired harmonics, A is the amplitude, f_f is the fundamental frequency and φ_k is the phase shift at each frequency. Setting n to infinity and all phase shifts to zero results in an ideal square wave.
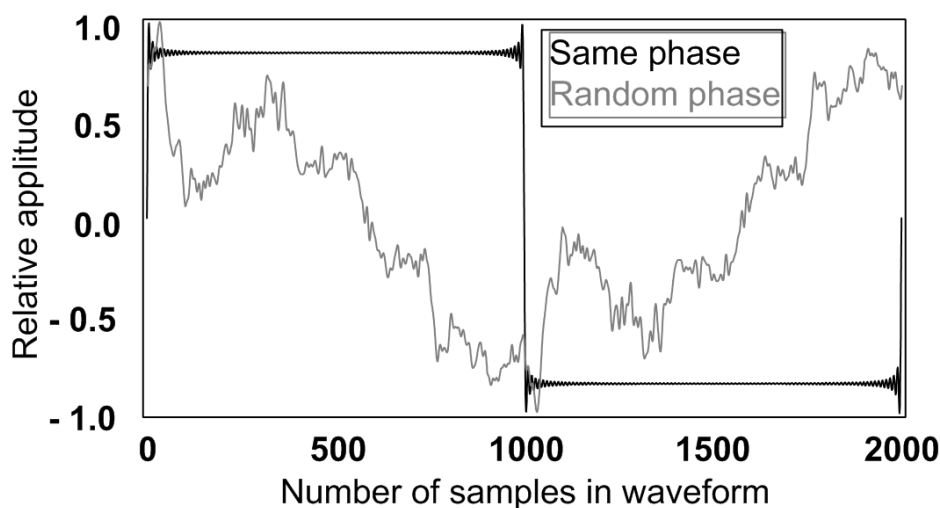
Two equivalent harmonics limited waveforms are shown in Figure 4.3. Both contain 100 odd harmonics. With all phases shifts equal to zero, a waveform similar to a square wave is obtained. However, the test waveform does not necessarily have to look like a square wave. With random phase shift for the harmonics, the gray waveform is obtained. The AWIS measurements will therefore provide the same results under these different waveforms. The harmonics limited waveform can be downloaded to the arbitrary waveform generator, which can generate a periodic voltage waveform with adjustable amplitude and fundamental frequency, f_f.

4.3 Test setup specification

To simplify the experiment setup, a 4.7 nF metalized polyester (PET) capacitor was used as the test object to represent the dielectric material. In order to match the impedance of the test object, a selected shunt device containing a 9 kΩ resistor in parallel with a 4.7 nF metalized polyester capacitor was employed. To record the voltage signals, the sampling rate of the DAQ card for each channel was set at 400 kS/s. One should notice that in order to achieve a broader frequency spectrum, the two grounded dummy channels needed for reducing the crosstalk (see section 3.3) were not implemented in this setup. However, an amplifier (OP42GP) was installed between the shunt and digitizer input for lowering the source impedance for the DAQ and further reducing capacitive crosstalk.

Calibration of the AWIS measurement system was performed by a 22 kΩ coaxial resistor, measured by an impedance analyzer (HP 4192A) in the frequency range from 25 Hz to 200 kHz. The average accuracy of this impedance analyzer is about 1 %, which might too low for precision measurement of unknown test objects. However, the accuracy of relative amplitudes of the same test object seems good enough for the comparison test waveforms.

4.4 Test results

In Figure 4.4, ten individual measurements obtained by AWIS under a square-wave waveform and a harmonics limited waveform are compared. A dramatic decrease of the variations, especially for the loss factor at high frequencies, is an apparent result when using the harmonics limited waveform. The reduction of variation indicates that aliasing was strongly affecting the square-wave results and the remaining variation from the harmonics limited waveform is due to the reduced signal to noise ratio at high frequencies.

The idea of using a specially adopted arbitrary waveform as test source in dielectric response measurement has been tried by other researchers as well. Some examples can be found in [48, 49].
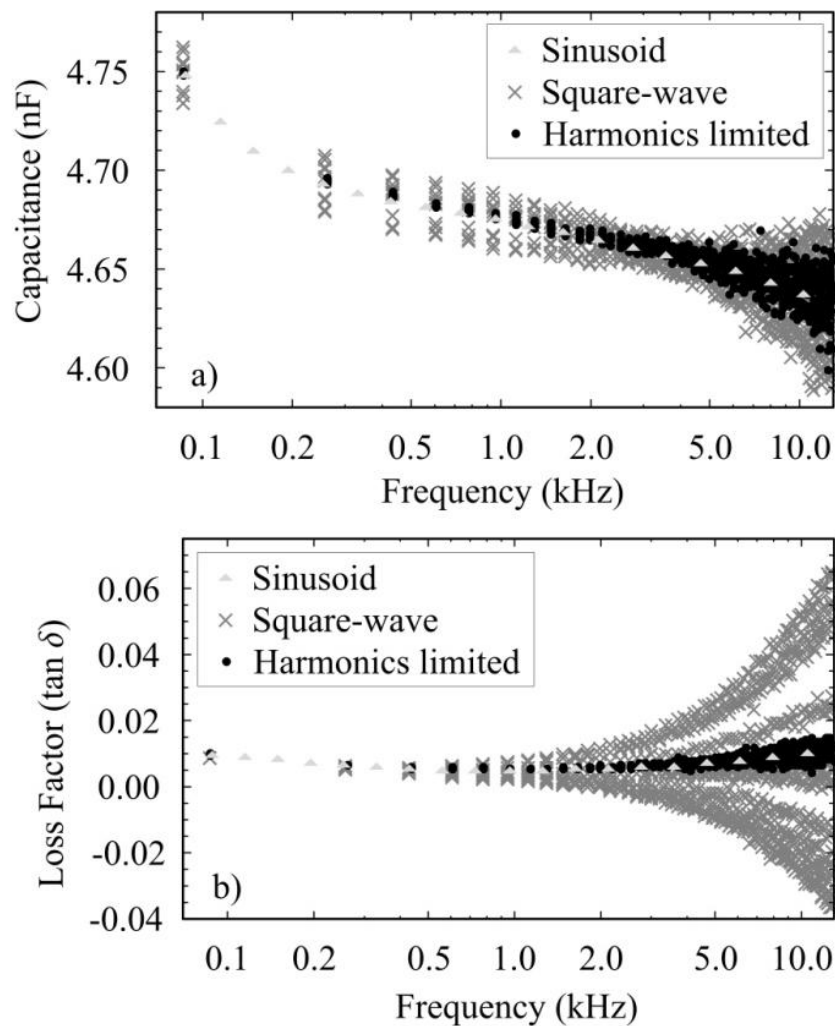

Figure 4.4: Comparison of ten individual measurements, a) capacitance and b) loss factor, obtained under a harmonics limited waveform (f_f = 80 Hz, 10331 samples in the waveform, 75 odd harmonics) and under a square-wave waveform (f_f = 80 Hz). As reference, a result obtained from swept measurement under sinusoidal waveform is shown.

4.5 Aliasing of harmonic groups

It was observed during the development work that when the fundamental frequency was varied by 1 or 2 Hz, the results became sometimes unstable. Of course, this disturbing factor had to be further investigated. By studying the full frequency spectra of a harmonics limited voltage waveform, several unexpected harmonic groups with different amplitudes were found, being evenly distributed over the spectrum.

These harmonic groups appeared due to the oscillator's sample generation rate, which is the number of samples in the arbitrary waveform multiplied with the fundamental frequency. In Figure 4.5, the full frequency spectrum of a harmonics limited waveform is shown.

Several harmonics groups with different amplitude appear in the spectrum. If the number of samples in the waveform is changed to 4000, all the harmonics groups are overlapped at 0 Hz as the sample generation rate is then the same as the Nyquist frequency. As a result, the noise level is increased 100 times as compared to the measurement with 4320 samples in the waveform. Thus, a similar effect as from the square-wave waveform is observed but now due to the aliasing of the sample generation rate and not of the fundamental frequency harmonics. Similar to Figure 4.2, the aliased folding sequence of the harmonic groups are marked in Figure 4.5.

The aliasing behavior of the harmonics groups have been studied in several tests with different fundamental frequency and number of samples in the waveform. They can be described by the following characteristics:

1) The width of each harmonics group is twice the desired frequency spectrum;

2) The frequency interval between neighboring harmonics groups is the oscillator's sample generation rate;

3) The amplitude attenuation of harmonics groups increases by increasing the number of samples in the waveform.
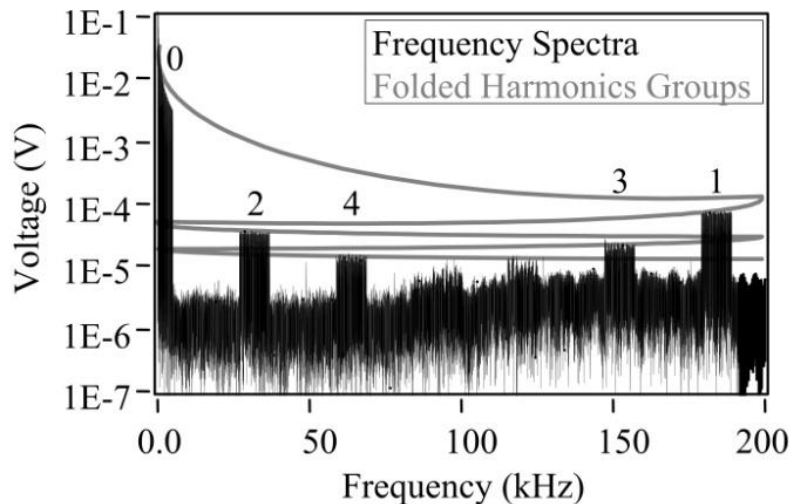

Figure 4.5: Frequency spectra of harmonics limited voltage waveform with folded harmonics groups (4320 samples in waveform, f_f = 50 Hz, 50 odd harmonics); DAQ card sampling rate: 400 kS/s, waveform generation rate: 216 kS/s.

4.6 Practical adaption

Equations 4.1 and 4.2 can be employed to predict this aliasing behavior of harmonic groups in order to find a proper waveform to avoid overlapping. With a specific fundamental frequency, f_f, and recording sampling rate, a favorable sample generation rate can be chosen by adjusting the number of data points in the waveform. Thus, the place of the folded-back harmonics groups in the spectrum can be controlled. There are two principles to follow when adjusting this number:

1) Placing as much low order harmonics groups away from the fundamental harmonic group frequency as possible;

2) Setting the number of samples in a waveform as high as possible in order to attenuate the harmonics groups better.

However, the number of samples is limited by the arbitrary waveform generator's capability; in this case a maximum 16000 points per period may be used.

Figure 4.6 illustrates a developed support tool that uses equations 4.1 and 4.2 to predict the position of folded-back harmonic groups. With this tool, the fundamental frequency, the number of samples in waveform definition and the sampling rate of the DAQ card can be adjusted to avoid interference from aliased harmonic groups in the desired frequency range.

As a consequence of the aliasing of harmonics groups, only about 10% of the frequency spectrum (up to 20 kHz with 400 kHz sampling rate) can be used effectively with a harmonic limited waveform. It will namely be more and more difficult to avoid overlap between the harmonic groups and the desired frequency range as the used portion of the available spectrum is increased. As the amplitude of folded-back harmonics decreases with the harmonic order, only a limited number of groups need to be considered, as seen from figure 4.5. A too low fundamental frequency will also limit the accuracy at high frequencies as a large number of harmonics is required. Therefore, the dielectric response measurements using harmonics limited waveforms show the expected accuracy in a frequency range from 50 Hz up to 20 kHz.
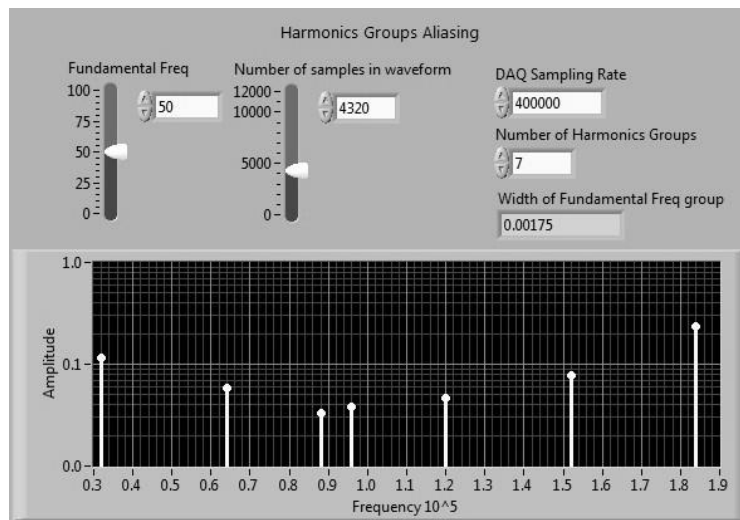

Figure 4.6: A support tool for predicting the position of folded-back harmonic groups with specified fundamental frequency, number of samples in the waveform and DAQ card sampling rate (the data from Figure 4.5 are analyzed).

4.7 Application - measurements under changing condition

To study dielectric properties over a board frequency spectrum often requires a certain time, a few minutes, to sweep the required number of frequencies. Dielectric properties are often strongly influenced by the environmental conditions for the material, such as, temperature, humidity, pressure, etc. If the condition is continually changing, the obtained results at different frequencies may therefore become difficult to compare.

Using harmonic limited waveform with AWIS technique enables us to determine an entire dielectric frequency response spectrum from one measurement. This ensures that all frequency points are measured under the same condition. Further, with continuous monitoring, the dielectric properties of a specimen or a system can be studied under changing environmental conditions.

A dry pressboard specimen was employed to demonstrate the dielectric response measurements under rapidly changing condition. The specimen was first dried and heated up to around 60 ⁰C and then placed into a test cell for cooling under normal room conditions. While the specimen was cooling, the measurements were carried out. This process was repeated several times for both swept measurements and harmonic limited measurements. Figure 4.7 illustrates the measured loss factor of the pressboard specimen under different temperatures. As a reference, swept and harmonic limited measurements, made under same stable room conditions, show close to identical characteristics. The measurements under the changing temperature, however, exhibit different dependences on frequency. As seen in the figure, in the swept measurement, the time needed to sweep the spectrum roughly equals the time required for the temperature to decrease from 60 ⁰C to room temperature (20 ⁰C), therefore, each swept frequency is measured at a different temperature. The harmonic limited measurement, however, obtains the whole spectrum from a single measurement and this ensures that each frequency point is measured at the same temperature. The results from harmonic limited measurements also show that the loss factor decreases with the temperature. The swept measurement indicates a much stronger loss decrease with frequency. This is because of the sweep direction, if frequencies were swept from high to low, a much flatter response would appear.
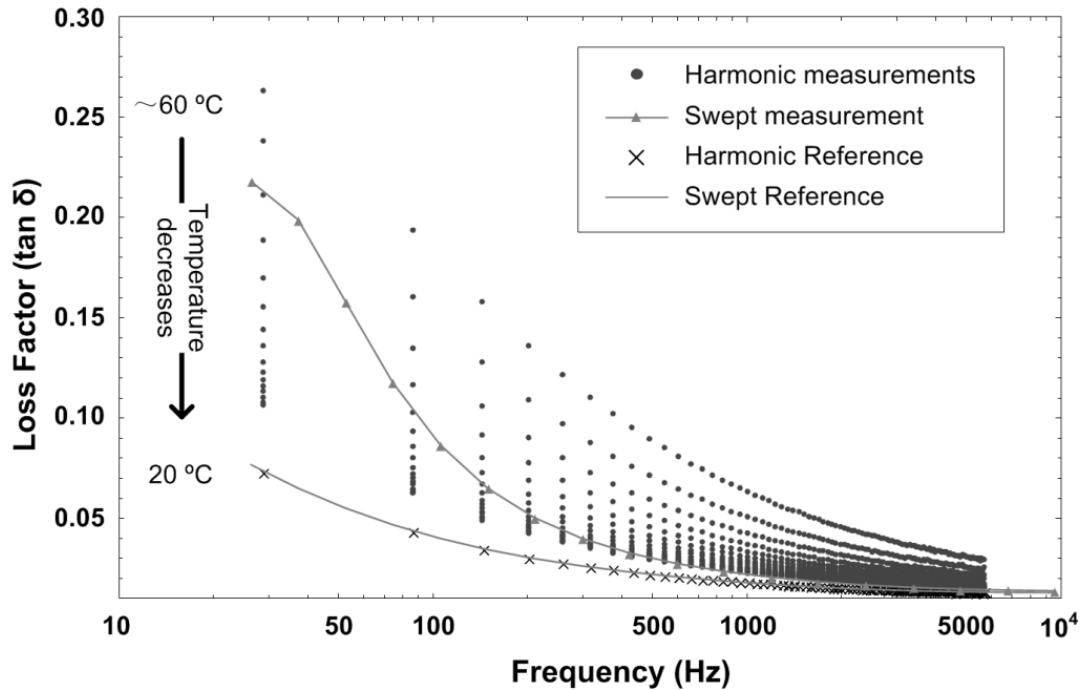
Figure 4.7: Frequency dependence of loss factor for dry pressboard sample measured under continuously changing temperature (from 60 °C down to 20 °C), the time interval between each swept frequencies point and between each harmonic measurement are the same, 5 seconds.

4.8 Summary

In this chapter, a harmonics limited waveform is presented that can be employed for precision dielectric response measurement with high time resolution and avoiding aliasing interferences. To fulfill these purposes, the generation of the harmonics limited waveform must take into consideration the fundamental frequency, the number of samples in the harmonics limited waveform and the sampling rate in the measurement. This was facilitated by the equations given in this chapter for the apparent frequencies of aliased signals.

The dielectric response measurements achieved with harmonics limited waveforms show the expected accuracy in a frequency range from 50 Hz up to 20 kHz. Further, the harmonics limited measurement is also exemplified by studying dielectric properties under rapidly changing environmental conditions.

5 Air Reference Method

An air reference method and a contact-free electrode arrangement are introduced in this chapter to enhance the dielectric characterization accuracy through avoiding the problems possibly arising when using different electrodes. It is shown that by performing a calibration with the electrode arrangement filled with air under the same conditions as the material specimen is tested, the air reference method can improve the measurement accuracy substantially. This type of approach also eliminates the need of a detailed modeling of the analog measurement circuit. In conjunction with the contact-free measurements, the approach allows for avoiding complicated and time-consuming specimen preparation procedures. Both the measurement methodology as well as the electrode arrangement are presented and evaluated using different dielectric response instruments and materials.

5.1 Contact-free measurement

The idea of a contact-free dielectric response measurement is to place a piece of a flat dielectric material specimen on the bottom electrode of a horizontal arrangement without a direct contact to the top electrode, as shown in figure 5.1. As there is no pressure applied from top electrode, a possible deformation of the specimen is avoided. Moreover, without any current paths on the surface of the tested specimen, influence of the surface conductivity is limited. Further, if the specimen area is smaller than the electrode area, field distortion at the electrode edge due to a presence of the test material becomes reduced but field distortion on specimen edges may affect the result.
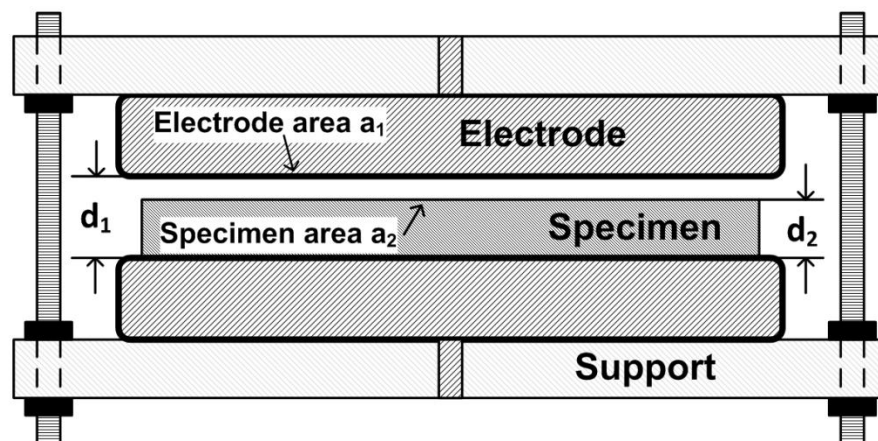

Figure 5.1: Sketch of the contact-free electrode arrangement, d_1 is the distance between two parallel electrodes and d_2 is the thickness of tested material, a_1 is the area of electrode and a_2 is the specimen area.

A partially filled test gap can be modeled by two in series connected capacitors (C_{topAir} and $C_{specimen}$) in parallel with a capacitor ($C_{sideAir}$), jointly resulting in a total capacitance as given by equation 5.1

$$C_{tot} = C_{sideAir} + \frac{C_{topAir}\, C_{specimen}}{C_{topAir} + C_{specimen}} \qquad (5.1)$$

where, $C_{specimen}$, C_{topAir} and $C_{sideAir}$ are the complex capacitances of the specimen, the air inside the electrode gap above the specimen (with area a_2 and distance d_1-d_2) and the air cylindrically around the specimen and the top air (with area a_1-a_2 and distance d_1). From equation 5.1, the specimen capacitance can be calculated if the dimensions and the total capacitances are known:

$$C_{specimen} = \frac{C_{topAir}(C_{tot} - C_{sideAir})}{C_{topAir} + C_{sideAir} - C_{tot}} \qquad (5.2)$$

If the inserted specimen area is larger than the electrode area ($a_2 > a_1$), the total capacitance as well as the specimen capacitance can further be simplified as:

$$C_{tot} = \frac{C_{air}\, C_{specimen}}{C_{air} + C_{specimen}} \qquad (5.3)$$

$$C_{specimen} = \frac{C_{air} C_{tot}}{C_{air} - C_{tot}} \qquad (5.4)$$

The air gap capacitances can be obtained from the air reference measurement, described in the next section, by correcting for the changed volume. Similar approaches were mentioned in [1, 2]. In this study we are however additionally using air as reference to calibrate the measurement instrument.

5.2 Air reference method

In the air reference method, one measures the complex capacitance of a test cell under the same frequencies and the same test conditions twice, with and without presence of the tested material. The complex permittivity of the tested material is then calculated from the ratio of the two measured complex capacitances and the knowledge of the tested material volume and dimensions of the test cell.

The first measurement is made on the capacitance (C_1) of two parallel electrodes (area a_1 and gap distance d_1) with only air in between. This measurement can than be looked as an air reference calibration. According to the literature, the relative permittivity of air under normal condition is $1.00058986 \pm 0.00000050$ [50] and the loss factor is assumed to be negligible but dependent on humidity. Therefore, for the present accuracy requirements, the relative permittivity of air can be set to unity with no losses. If the required accuracy is higher, the measurements can be made in vacuum. In practice, it is not necessary to perform this air calibration measurement for every specimen characterization, but it should preferably be done when the testing conditions change, such as when the current shunt impedance shows drift, the distance between the electrodes is modified, the testing cell is moved or the temperature varies.

The second capacitance (C_2) is the capacitance of the identical test cell as in the first calibration measurement but with a material specimen (thickness d_2, $d_2 \leq d_1$) in the electrode gap. The

capacitance C_2 is given by C_{tot} of equation 5.1 or 5.3. Together with the first measured air capacitance C_1, the complex permittivity and dissipation factor of the material can be calculated through equation 5.5

$$\varepsilon_r = \frac{d_r(K+a_r-1)}{d_r(K+a_r-1)-K+1} \tag{5.5}$$

where $K = \frac{C_2}{C_1} = \frac{Z_1}{Z_2}, a_r = \frac{a_2}{a_1}, d_r = \frac{d_2}{d_1}$

Again, if the specimen area is larger than the electrode area $(a_2 > a_1)$, the calculation for the complex permittivity can be further simplified as:

$$\varepsilon_r = d_r \frac{C_{specimen}}{C_1} = \frac{d_r K}{(d_r-1)K+1} \tag{5.6}$$

Here, C_1/d_r is the partial capacitance of the air volume that is replaced by the specimen.

Though it is not possible to characterize the current shunt impedance (Z_{sh}) in fine detail, the material permittivity can still be calculated with precision as the impedance ratio (K) from the two measurements is used in equation 5.5 and 5.6. From equation 3.1, it follows that the result does not depend on the shunt impedance if the same current shunt is used in both measurements. This does not mean that the shunt characteristics are unimportant, however. The shunt impedance is decisive for the signal to noise ratio and thus determines the resolution of loss factor measurement. A thermal drift causing a shunt impedance to change is here a main error source.

5.3 Measurement design

A contact-free electrode arrangement using the air reference method can be utilized by any dielectric response instrument with enough high resolution. As the air reference method eliminates detailed modeling of the analog circuit, this calibration principle can also be beneficial with contact electrode arrangements, where it may improve accuracy. Thus, two different instruments, AWIS and a commercial instrument, IDAX, were used to verify this method with both contact and contact-free electrode arrangements. As a comparison, the direct method is also used in IDAX measurements with a contact electrode arrangement.

5.3.1 Experimental setup

The air reference method is applied for both AWIS and IDAX measurement systems. The IDAX instrument (IDAX-300) [23] is a commercial insulation diagnostic analyzer. It applies a sinusoidal voltage with the desired frequency over the specimen and by accurately measuring the voltage and resulting current, the total impedance is obtained. At this level of abstraction, both AWIS and IDAX operate similarly. The main practical difference between them is that IDAX provides its own test voltage source and accurate provisions with electrometer (operational amplifier), feedback capacitor and balancing capacitor for signal measurements [14]. AWIS, on the other hand, is more a concept than an instrument and therefore we have to arrange a suitable voltage source and select appropriate and practical measurement provisions. This means that AWIS can better be optimized for a specific measurement, for example, when using harmonic limited waveforms.

The used AWIS setup consists of a 15 MHz arbitrary waveform generator (HP 33120A) which provides the applied voltage V_0, a shunt (Z_{sh}) which converts the current response into a measureable voltage V_1, the test object (Z_{to}), and a 16-Bit, 1.25 MS/s multiplexing DAQ card (NI USB-6251) which is used to measure V_0 and V_1. The sampling rate of the DAQ card is set to 200 kS/s. To ensure low source impedance for the current measurement, which is required with multiplexing DAQ cards, the V_1 signal is passed through a buffer amplifier, the basic measurement circuit can be found in figure 3.12.

The current shunt (Z_{sh}) is built by a capacitor in parallel with a resistor. The advantages of a capacitive shunt are discussed in section 3.2.

The used IDAX instrument is an insulation diagnostic system mainly intended for analysis of power apparatuses but it may also be used for material characterization. Sinusoidal voltages up to 200 V_{peak} in the frequency range from 0.1 mHz to 10 kHz can be applied to the test object. According to the manual [23], the accuracy of the IDAX-300 instrument for capacitance measurement is 0.5% + 1 pF and the accuracy of the loss factor from 1 mHz to 100 Hz is 1% + 0.0003, from 100 Hz up to 1 kHz is 2% + 0.0005. The loss factor accuracy from 1 kHz up to 10 kHz is not specified in the manual.

In each IDAX measurement, one pre-measurement is performed to select among several current sensitivities for different frequency bands in order to obtain optimal response amplitude. For the AWIS measurements, there is no need to change shunt because of its high sensitivity and the capacitive shunt arrangement.

The used test cell is made up of two flat bare stainless steel electrodes (r = 47 mm) which are supported by two plexiglass plates and three screws, as shown in figure 5.1. The distance between the two electrodes can be adjusted by modifying the position of nuts on the screws. The test cell is fixed in a shielded metal box to minimize the external interferences.

5.3.2 Measurement circuit characterization

In the frequency range from 10 Hz up to 10^5 Hz small stray capacitances and line inductances will influence results of the measurements significantly and are not possible to eliminate from the circuit.

Even though a detailed knowledge of the shunt properties is not required when the air reference method is used, it is important to verify that the gross properties are as desired. Figure 5.2 shows the properties of the used shunt, as calculated from a measurement with the air filled test cell. It is assumed that the cell is a loss-free air capacitor. For comparison, a model of the shunt with the nominal values of the components (330 pF // 900 kΩ) and assuming 1% loss factor in the shunt capacitor at all frequencies is also shown. The tendencies in frequency dependences of the measurement result and the model are similar, though disparities are apparent in the shape of the decreasing part, likely due to frequency dependence of the shunt capacitor losses. There is further a significant difference in the parameter values at low frequencies. According to datasheets of the shunt components, the capacitor has 10% tolerance and the resistor has 5% tolerance. Even if the maximum variations from the nominal values are taken into account, additionally 2% less resistance and 7% more capacitance are found in the measured shunt. This clearly indicates that other circuit components are contributing to the shunt impedance, such as capacitances of connecting cables and the input impedance of the DAQ card.
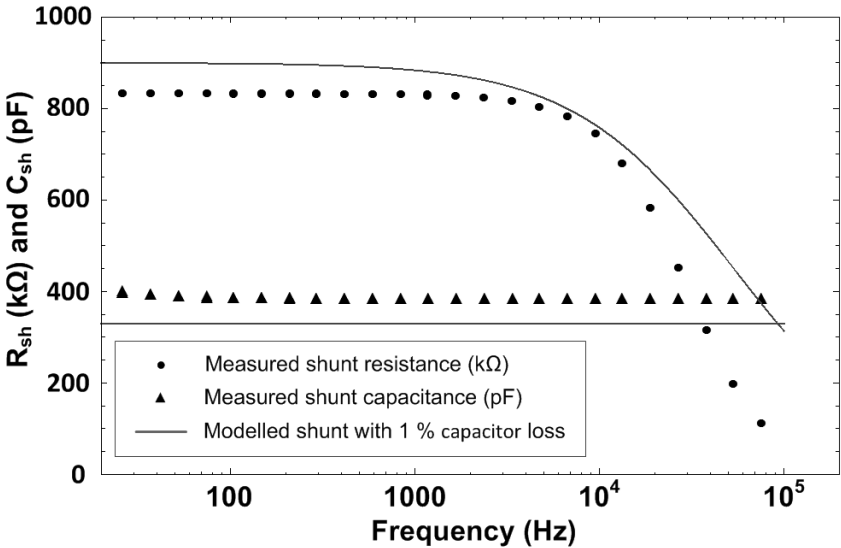
Figure 5.2: Measured and modeled shunt resistance and capacitance of the AWIS setup, modeled shunt circuit with nominal value of shunt components, including 1% shunt capacitor loss, is used.
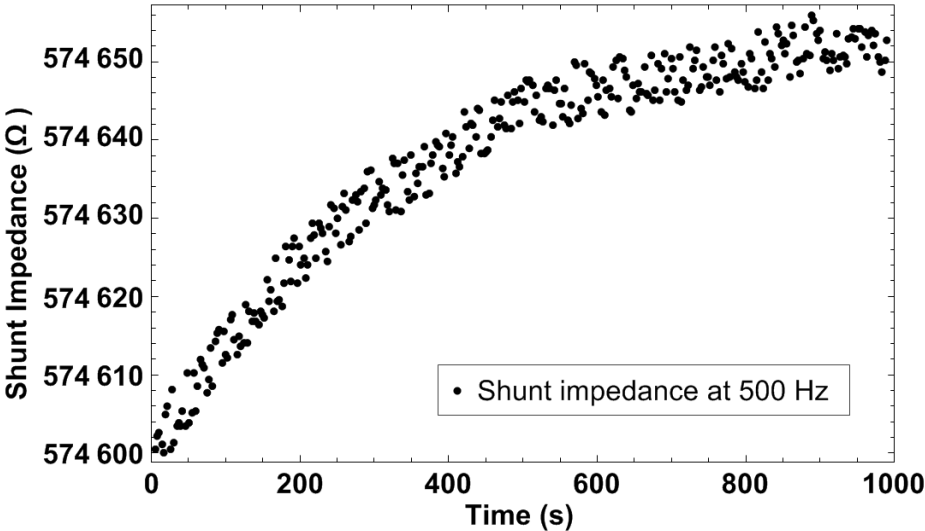
Figure 5.3: Measured impedance of current shunt at 500 Hz during 1000 seconds at constant current load. The noise level is visible by the distribution of individual measurement points

Since detailed shunt modeling is avoided in AWIS measurement when the air reference method is applied, the bottleneck in high precision dielectric response measurement is the shunt impedance variation due to its heating by the flowing current. An example on how the shunt used in this work behaves in such situations is illustrated in figure 5.3. One may clearly see that at least 1000 seconds are needed for the impedance to stabilize. During this time, the change of the shunt impedance is about 5 times the noise level. Here, it is clearly favorable to perform a calibration

when the instrument has stabilized under the correct current load and other ambient conditions, which is made possible by the air reference method.

5.3.3 Measurement procedure

The relative permittivity and loss factor as function of frequency are calculated from the AWIS and the IDAX measured results using both contact and contact-free electrode arrangements.

In the AWIS measurements, the air reference method has to be used for both contact and contact-free electrode arrangements, as the current shunt is not characterized. Therefore, the impedance ratio (K) is obtained from the applied and response voltages (V_0 and V_1) by equation 3.1, and thereafter is used in equation 5.5 or 5.6 to calculate the complex permittivity of the material.

In the IDAX measurements, the ratio of the two measured complex capacitances (C_1 and C_2) is directly used in equation 5.5 or 5.6 to calculate the complex permittivity of the material by the air reference method with both contact and contact-free electrode arrangements.

The traditional, direct dielectric response measurement with contact electrode arrangement can also be performed with the IDAX instrument. The relative permittivity and loss factor are then directly calculated from the measured specimen capacitance (C_2) and the dimensions of the test cell.

5.3.4 Surface charge interferences

Due to presence of the air gap between specimen surface and electrode, any charges deposited on the specimen surface cannot be neutralized by the electrodes as in traditional contact arrangements. Neutralization of surface charges by bulk or surface conduction and charge exchange with air are often slow processes for modern insulation materials. Further, due to contamination and roughness of the specimen surface, the deposited charges on the surface are often not in equilibrium and may influence the apparent losses.

The impulse response of the shunt used in AWIS setup is characterized by a fast rise time and an exponential decay with a time constant given by eq. 3.1. Thus, all fast current pulses will appear in the frequency range below the corner frequency of the shunt which is $1/(2\,\pi\,\tau)$. With the present shunt, this is about 500 Hz. Therefore, if the specimen surface is charged and the charges may eventually move, this will always be detected as low frequency currents. As these currents are not related to the dielectric properties of the specimen, they may cause measurements errors. It is interesting to note, however, that the frequency range above the corner frequency of the shunt will be free from such errors. This is illustrated in figure 5.4, where noise levels at low frequencies of the measured responding voltage V_1 are significantly larger than at other frequencies in the spectrum as well as larger than the noise level of applied voltage V_0.

The consequence of surface charge presence in the contact-free measurement is that measured losses in the low frequency range are increased. It is illustrated in figure 5.5, in which polycarbonate specimen was measured twice by applying the air reference method with contact-free electrode arrangement and an identical test gap. The only difference between the two measurements is the specimen surface condition. In the first measurement, the specimen was rubbed against hair to charge the surface, whereas in the second measurement, the specimen was cleaned by flushing with isopropanol and dried under room conditions. The figure shows clearly that the losses of the specimen with surface charges are significantly larger than with a cleaned surface at low frequencies and the shape of the curve is very irregular. Additional measurements

indicated that the losses of the charged specimen were not repeatable. Therefore, any electrostatic charges on the specimen surface need to be removed to enable reproducible measurements. Though the results in figure 5.5 show a significant difference between charged and cleaned polycarbonate specimen, this difference may not be critical if high loss materials are tested, for example pressboard. Pressboard has a loss factor in the range of percent and the influence of the surface charges is at least ten times smaller.
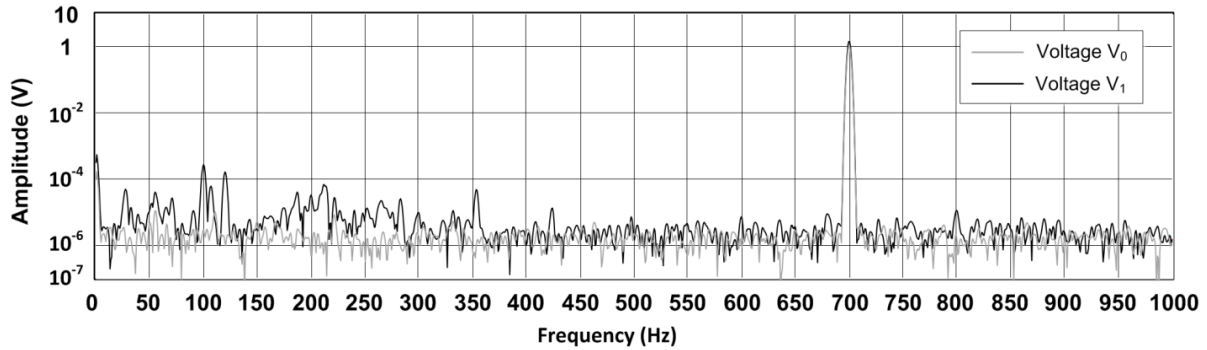
Figure 5.4: Measured frequency spectrum of applied voltage V_0 (7 V and 700 Hz) and its responding voltage V_1 from a polycarbonate specimen with charged surface in contact-free electrode arrangement.
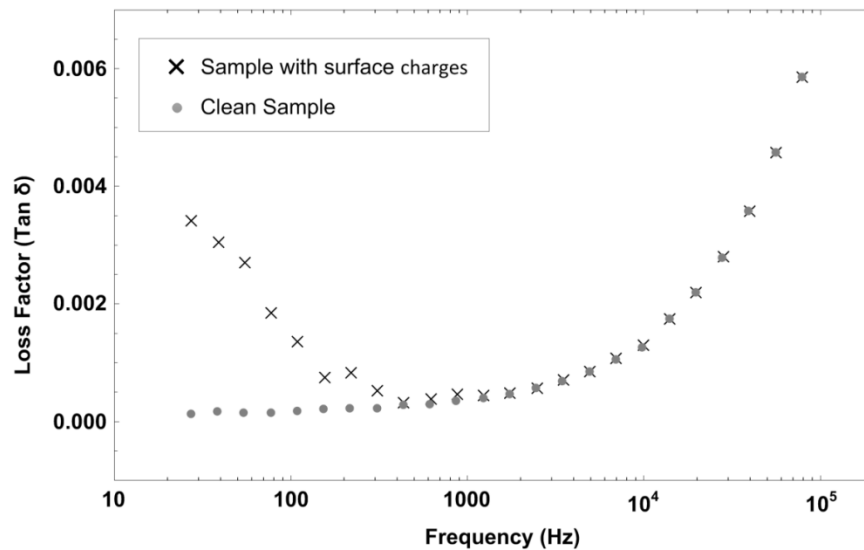
Figure 5.5: Results of two measurements of losses of a polycarbonate specimen with the same test gap using air reference method in contact-free electrode arrangement. In the first measurement, specimen was rubbed against hair to charge the surface; in the second measurement, specimen was cleaned by flushing the surface with isopropanol.

5.4 Error analysis and estimation

In this section, both error analysis and error estimation are carried out and discussed. The error analysis is based on the theoretical approach by identifying possible error sources in the measurement procedure and analysis of error propagation consequences in general, whereas the error estimation is to process the actual measured data sets by accounting for the uncertainty range of critical parameters. It has been verified that both the approaches yield similar results.

5.4.1 Error analysis

The permittivity and loss factor resolutions will be degraded by the existence of the air gap. This accuracy loss can be quantified by analysis of the error sources of the contact-free electrode arrangement with respect to the contact measurement.

From equation 5.6, two error sources can be identified. One is the distance measurement error which will be present in d_r, another error source comes from the electrical measurement noise and drift which will be present in the complex K measurement. Here, one should note that the drift in amplitude and angle of K are not always the same therefore they should be considered separately. The use of air reference method eliminates voltage and current sensing errors, which otherwise must be considered in standard approaches.

With these two independent error sources, the resulting error in permittivity is calculated as

$$\Delta(\varepsilon_r) = \left|\frac{\partial \varepsilon_r}{\partial d_r}\right| \Delta(d_r) + \left|\frac{\partial \varepsilon_r}{\partial K}\right| \Delta(K) = \delta_d \Delta(d_r) + \delta_K \Delta(K) \qquad (5.7)$$

where $\Delta(d_r)$ and $\Delta(K)$ are distance measurement and electrical measurement error estimates respectively, δ_d and δ_K are sensitivity parameters. Distance measurement errors influence however also contact measurement. Therefore a proper evaluation of the error increase due to contact free measurements should only consider the error increase due to the air gap $\hat{\Delta}(\varepsilon_r)$, which is found by forcing the sensitivity parameters to unity when $d_r=1$:

$$\hat{\Delta}(\varepsilon_r) = \hat{\delta}_d \Delta(d_r) + \hat{\delta}_K \Delta(K) \qquad (5.8)$$

$$\hat{\delta} = \delta(d_r)/\delta(d_r = 1) \qquad (5.9)$$

thus defining the normalized sensitivity parameters $\hat{\delta}$.

An expression for the error increase due to distance measurement error, δ_d, as defined by equation 5.7, can be found from equation 5.6 by first differentiating by d_r and then substituting K with ε_r:

$$\delta_d = \frac{(\varepsilon_r-1)\varepsilon_r}{d_r} \qquad (5.10)$$

Here it is clear that there is an error increase also at $d_r=1$ due to the permittivity. The noise sensitivity parameter, δ_K, is found from equation 5.6 in the same way.

$$\delta_K = \left|\frac{\partial \varepsilon_r}{\partial K}\right| = \frac{((1-d_r)\varepsilon_r+d_r)^2}{d_r} \qquad (5.11)$$

This is unity at $d_r=1$, reflecting that the noise influence is the same for all permittivity values in contact measurements.

A similar analysis can be performed for the error increase in the loss factor, $tan\delta$. This is slightly more complicated by the need for separation of the real and imaginary parts of K, as illustrated in equation 5.12, but otherwise very similar. As the resulting expressions are quite complicated, these are not presented here. However, for low loss factors, the result is approximately the same as in equation 5.11.

$$\delta_K(tan\delta) = \left|\frac{\partial tan\delta}{\partial Re[K]}\right| + \left|\frac{\partial tan\delta}{\partial Im[K]}\right| \tag{5.12}$$

To exemplify the error increase magnitudes, the normalized sensitivity parameters for some selected permittivity values (1, 3, and 5) are presented in figures 5.6 and 5.7.

As illustrated in figure 5.6, the increase in ε_r and $tan\delta$ errors due to distance ratio measurement error $\Delta(d_r)$ relative to the contact measurement increases with decreasing distance ratio d_r and they are independent on ε_r.

The second error source, electrical measurement noise and drift, causes error increases as illustrated in figure 5.7. In this case, the increases in both permittivity and loss are ε_r dependent. As a worst case, an order of magnitude in precision may be lost for a half filled electrode gap with materials of interest.

Even though the contact-free air reference method will amplify the errors from both distance and electrical measurements, the elimination of the sensing circuit characterization is a major error-reducing factor. In some cases, especially for small losses, systematic errors in the sensing characterisation dominate the loss factor error, as will be exemplified below. This is because it is very difficult to characterise electrical components with a precision of 0.01 % or better.

The total error in the contact-free measurement can thus be calculated using the estimated specimen permittivity and calculated noise sensitivity as described above.
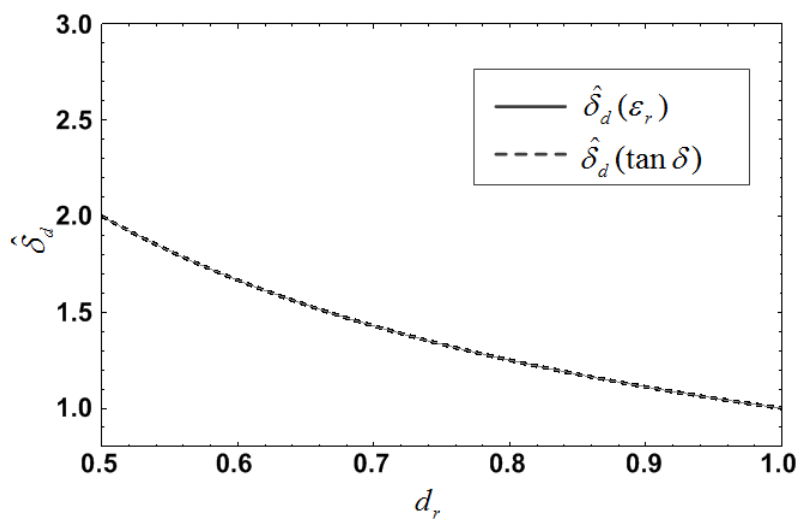

Figure 5.6: Normalised distance sensitivity parameter, $\hat{\delta}_d$, as a function of gap fill factor, d_r. The results for ε_r and $tan\delta$ are the same irrespective of the vaule of ε_r.
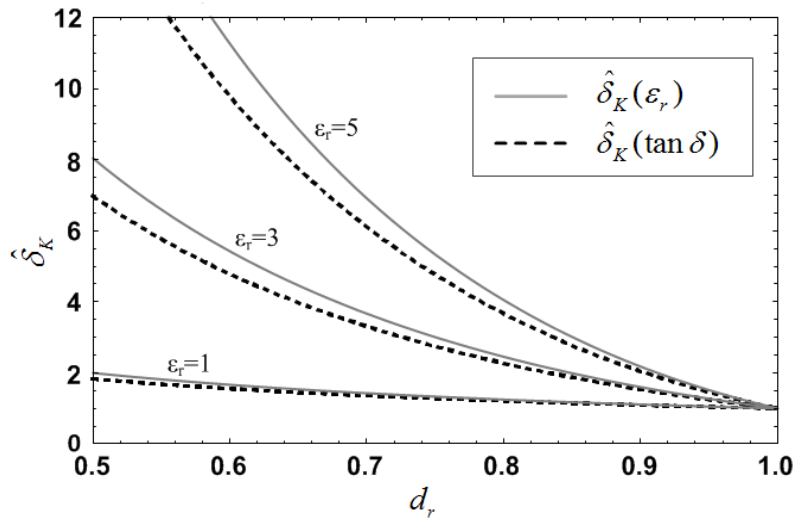
Figure 5.7: Noise sensitivity parameter, $\hat{\delta}_K$, as a function of the gap fill factor, d_r. The solid lines are valid for ε_r and the dashed lines for $tan\delta$, with ε_r = 5, 3, 1 from top of the figure. In the figure, a loss factor level of 10% is used to make the difference visible. Already at 1% the curves for ε_r and $tan\delta$ are almost identical.

5.4.2 Error estimation

Error estimation in practical measurement is performed based on the original measured data with a set of values for the critical parameters that cover the estimated uncertainty range. The two identified error sources which define the error range are estimated as discussed below.

The distance measurement error can be estimated by the accuracy of the instrument used for its determination, the distance of the test gap and the thickness of specimen. In our measurements, a micrometer with an accuracy of 0.005 mm is used.

The base error due to electrical measurement noise and drift can be estimated by measuring one identical electrode air gap twice and performing the air reference calculation. By repeating this measurement procedure several times, the deviation of air permittivity and loss factors can be taken as a measure of the error. Figure 5.8 shows the results of air permittivity and loss factor measured by air reference measurements with three different gap distances, each air gap was swept 5 times. The results indicate that the base error due to electrical measurement noise and drift is about $\pm$ 0.01% in permittivity measurement and in tan δ measurement $\pm$ 0.005% for both AWIS and IDAX instruments. As indicated in the manual, IDAX is less precisely calibrated above 1 kHz, which is visible in the loss factor plot of figure 5.8. Thus, the real error due to electrical measurement noise and drift can be estimated by performing the analysis several times using values of d_r and K within the uncertainty range.

A formal error analysis, as presented in section 5.4.1, provides the possibility to analyse error propagation consequences in general, as illustrated in figures 5.6 and 5.7 above. This is of great value, especially when designing a measurement. For practical measurements however, error estimates on actual data sets, a simpler and more direct method is to process the original data with a set of values for the critical parameters that cover the estimated uncertainty range. Such an

approach further serves as a confirmation of the formal error analysis. It has been verified in the measurements that both the error analysis and the error estimation methods provide similar results.

In these considerations, we have neglected an aspect that will cause some systematic errors in the permittivity estimations. When material specimens of different permittivity are to be measured, the effective electrode area will namely change due to distortion of the electric field at the electrode edges. To some extent, this effect can be controlled by geometric factors such as the electrode edge radius, electrode area to distance ratio and introduction of guard rings. For precision measurements of the permittivity, the edge field distortion needs nevertheless careful consideration and is therefore the subject of chapter 6.
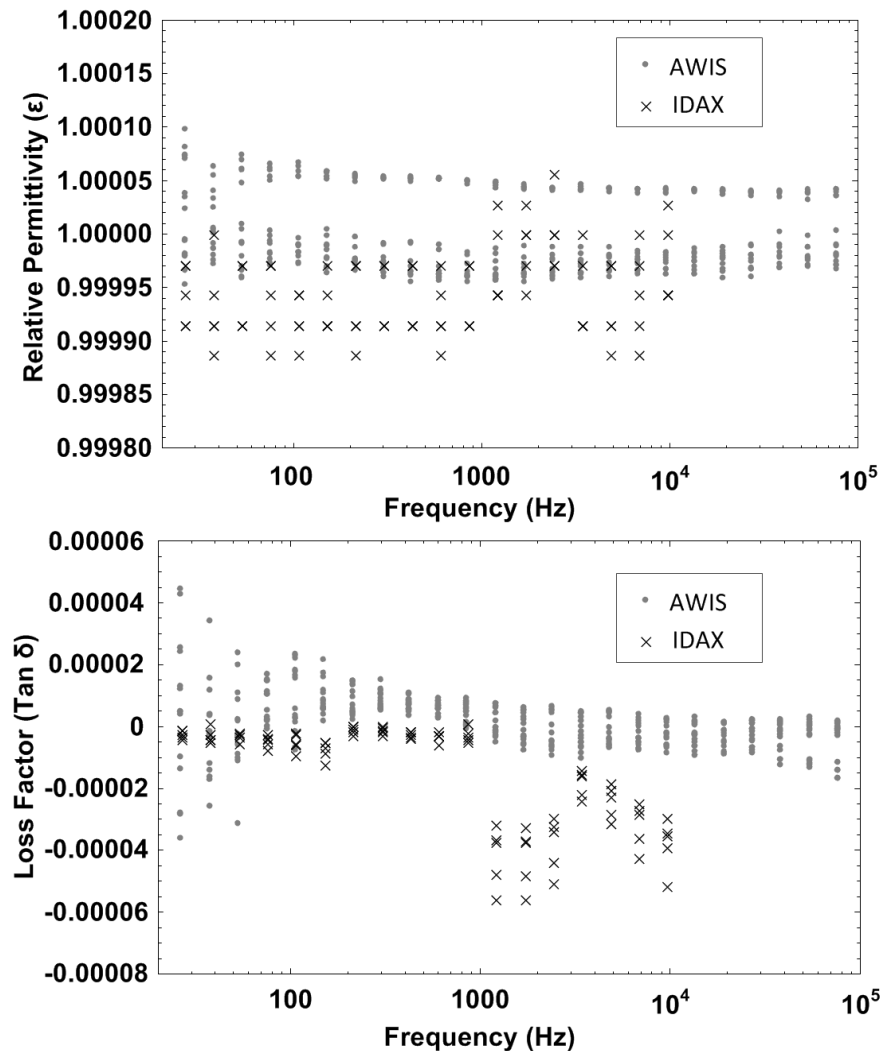

Figure 5.8: Relative permittivity and loss factor of air determined by air reference method with 3 different gap distances. These results indicate that base errors due to electrical measurement noise and drift in permittivity measurements are $\pm 0.01\%$ and in tan δ measurements $\pm 0.005\%$ for both AWIS and IDAX instruments.

5.5 Results of contact-free measurements

An absolute verification of the improved measurement accuracy by the air reference method is difficult to obtain. This would require comparison to an independent measurement method of high precision. For the loss factor, a calorimetric method could be considered, for example. Such methods are however at least as intricate as the proposed method and they need verification. As no such method is at present available to us, we had to resort to comparisons using different FDS instruments and materials to, at least, obtain an indication of measurement precision.

In contrast, the contact-free electrode arrangement can easily be verified by a comparison with a contact measurement. In such a comparison, increased losses in the contact measurement are expected at higher frequencies due to the possible existence of series resistances which should cause losses to increase linearly with frequency.

Two dielectric materials, polycarbonate and aluminum tri hydroxide (ATH) filled ethylene-propylene-diene-monomer (EPDM) rubber are used to exemplify the air reference method in application of the contact-free electrode arrangement. These materials have very different properties, EPDM rubber is much softer than polycarbonate. For comparisons, specimens were also measured by the direct method with contact electrode arrangement. Before each measurement, specimens were washed by isopropanol and left to dry under room conditions for one hour.

The errors in specimen measurements are then estimated based on the noise and drift observed in the air reference measurement as well as the estimated error of distance measurement.

5.5.1 Polycarbonate

The specimen was a 0.75 mm thick polycarbonate specimen, Bayer's GP 0099. It is a comparatively stiff material with polished surface. According to the material datasheet [51], the loss factor of the specimen is 0.0005 at 1 kHz, which is roughly the IDAX claimed accuracy level.

The relative permittivity and loss factor results of the specimen measured with the air reference method are shown in figure 5.9. As a comparison, results directly obtained by IDAX are also shown. The estimated error range for each measurement is also indicated in the figure. A good agreement is found between the results of relative permittivity values obtained by means of the two different instruments when applying the air reference method, while slightly different results may be noticed for the results obtained directly by IDAX. This difference is however within the sensing error range. The error estimation indicates that errors in permittivity measurements with contact electrode arrangement are roughly the same for both direct and air reference methods. A good agreement is also found in the results of loss factor measured by the air reference method. However, a significant difference is exhibited between the results from the air reference method and the IDAX directly measured loss factor. From the error estimation, it is seen that the air reference method has much less error than the direct method. This can be taken as an indication of accuracy improvement provided by the air reference method due to elimination of the sensing characteristics which dominate the direct measurement.

It has been noticed in our experiments that the sensitivities of IDAX and AWIS are different. In order to measure losses in the 0.1% range, AWIS needs a lower level of excitation voltage than IDAX, 7 V and 200 V were respectively needed for reaching this accuracy.

Figure 5.9: Relative permittivity and loss factor of 0.75 mm thick polycarbonate specimen measured by AWIS with the air reference method and measured by IDAX with both the air reference method and the direct method in the contact electrode arrangement. In order to improve the readability, only few data points are marked with error bars as they are in a same uncertainty range for each frequency.

The polycarbonate specimen was also measured with the contact-free electrode arrangement with an electrode distance of 1.5 mm. In figure 5.10, the relative permittivity and loss factor results are compared with the results obtained from the contact measurement.

A small difference is visible in the permittivity results, most probably related to effects of the effective electrode area. This difference is the subject of our further investigations in chapter 6. The error estimation shows that errors in permittivity measurements with contact-free electrode arrangements are larger than the error range of contact measurement as only half of the air gap was filled with the specimen. It is also interesting to note that the loss factor values of the contact-
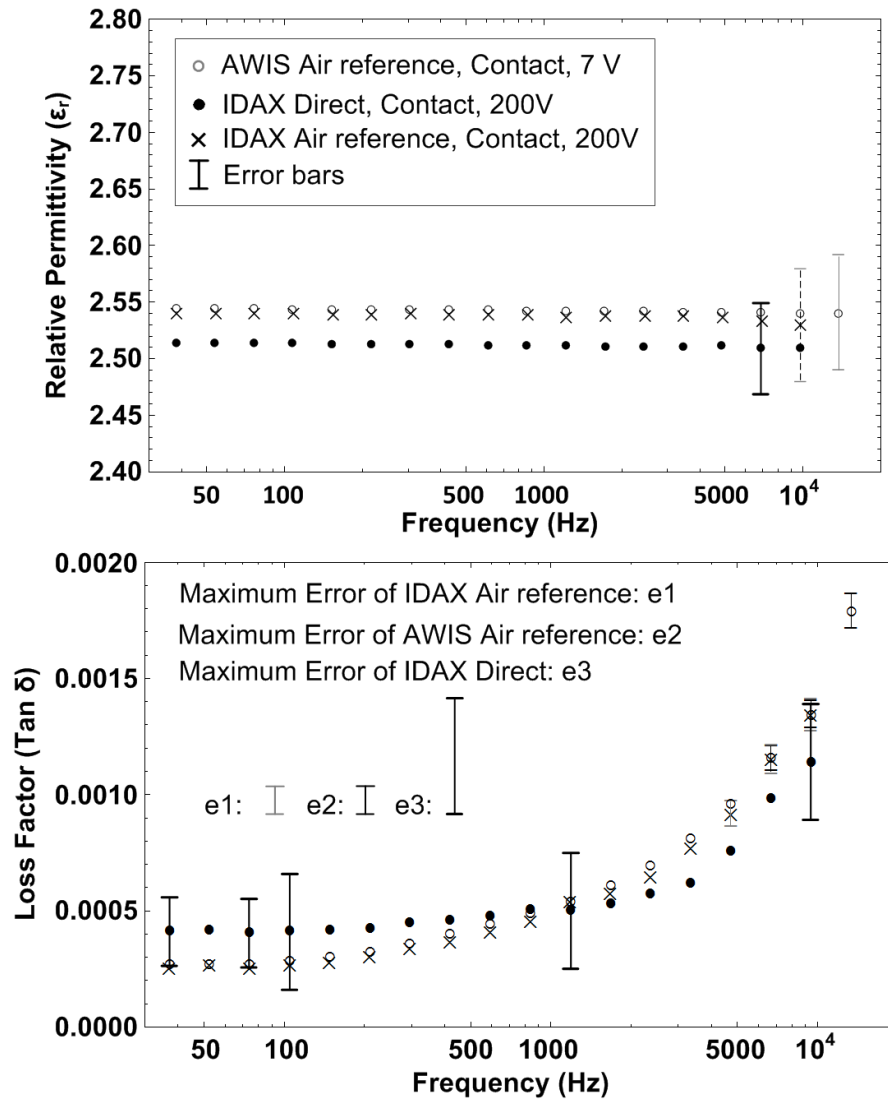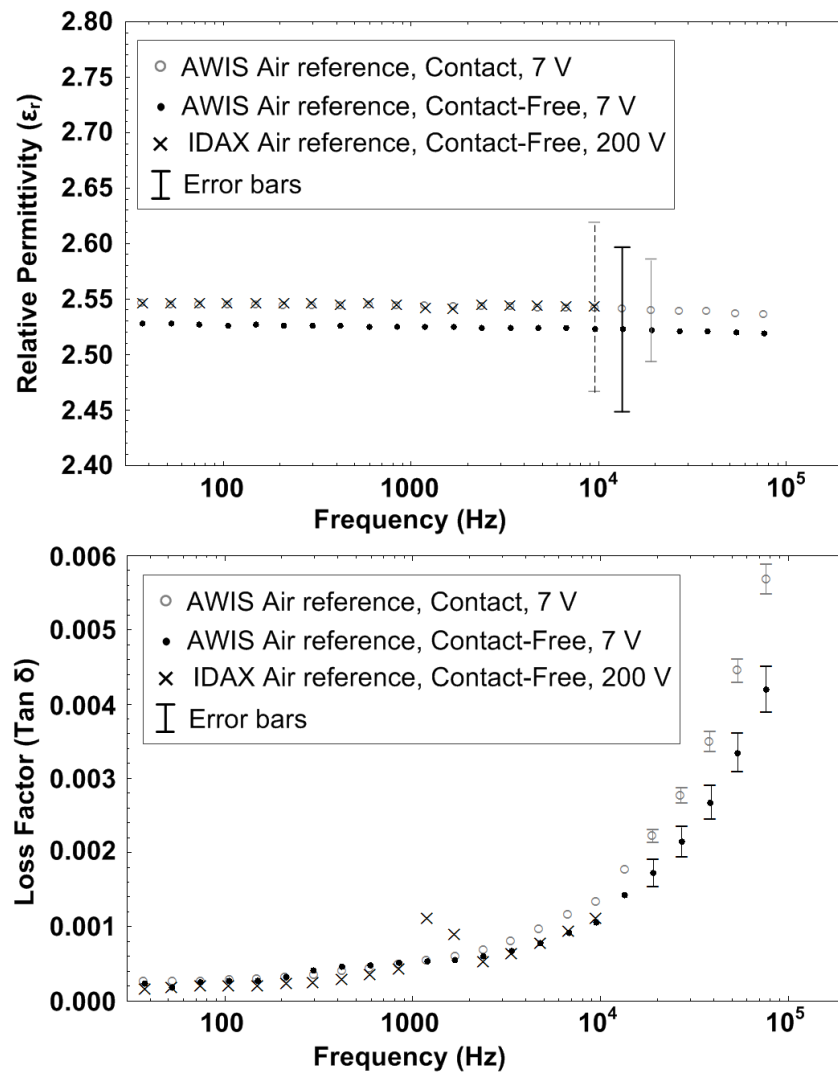
Figure 5.10: Relative permittivity and loss factor of a 0.75 mm thick polycarbonate specimen measured by AWIS with contact and contact-free electrode arrangement and measured by IDAX with contact-free electrode arrangement, similarly to figure 5.9. In the measurements the air reference method was applied.

free electrode arrangement are lower than the results obtained with the contact electrode arrangement, especially at higher frequencies. This effect is expected to arise from the existence of a series resistance at the specimen surface, and is thus taken as an indication, but not a proof, of increased precision by the contact-free measurements. The results also indicate that the error range for contact-free measurement is larger than the error range of contact air reference measurement but smaller than the difference due to the specimen surface contact.

In the loss factor results, two frequency points in the IDAX results deviate strongly from the overall trend. The reason for this deviation can be due to the automatic change of current sensitivity in IDAX. To use the air referencing method, it must be ensured that the same sensing

characteristics are used in both measurements at each frequency. If not, the error is only limited by the sensing accuracy, which may be much larger than the error from noise and drift.

5.5.2 EPDM with ATH filler

To further evaluate if the air reference method and the contact-free electrode arrangement are useful for characterizing of dielectric materials with different properties, an ATH filled EPDM rubber was also tested. This specimen had a thickness of 1.93 mm and the surface roughness $R_a < 5$ µm, $R_z < 10$ µm according to Dektak profilometer measurement [52].

The specimen was measured with the air reference method in both contact and contact-free electrode arrangements with an electrode distance of 2.57 mm.

In figure 5.11, loss factors of the two AWIS results are compared. As a reference, the IDAX measured result is also shown. Agreement is found in the results obtained with the contact electrode arrangement by AWIS and IDAX. The results with the contact-free electrode arrangement exhibit again a slightly lower loss factor as compared to the results with contact electrode arrangement, probably due to the influence of surface resistances. Thus, these results show similar behavior as the ones obtained on polycarbonate specimen.
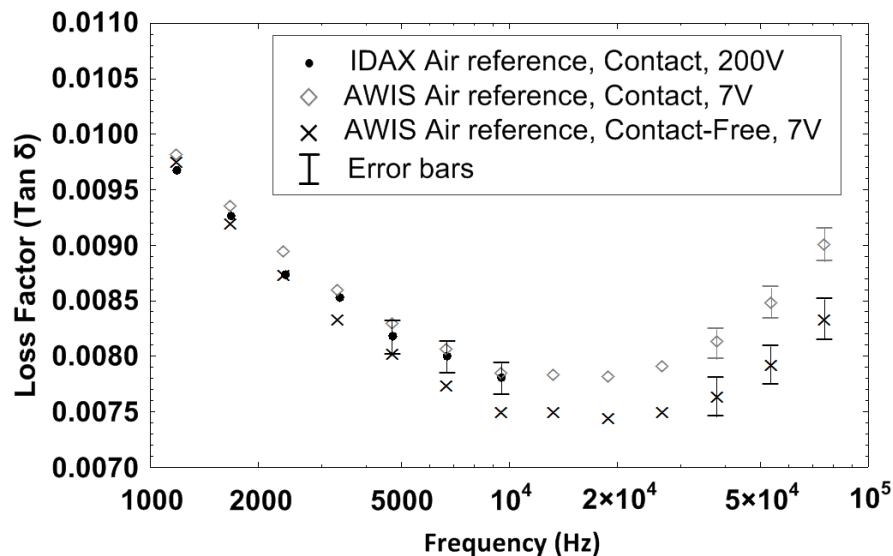

Figure 5.11: Loss factor of 1.93 mm thick EPDM with ATH filler specimen measured by AWIS and IDAX with different electrode arrangements, similarly to figure 5.9. In all the measurements, the air reference method was applied.

5.6 Further applications - fast dielectric material characterization

With the help of harmonic limited waveforms and the developed support tool, the most effective test waveform can be selected to determine dielectric properties of material over a broad frequency spectrum from a single measurement. The accuracy of such measurements can further be improved by implementing the contact-free electrode arrangement with the air reference method. In this section, combination of harmonic limited waveform and the air reference method is implemented in the contact-free electrode arrangement for a fast dielectric material characterization.

A 1.93 mm ATH filled EPDM rubber was first measured in a 2.59 mm test gap by AWIS with both swept sinusoidal and harmonic limited waveform. Then, the specimen was measured again by IDAX with traditional sinusoidal swept method and contact electrode arrangement. In Figure 5.13, obtained relativity permittivity and dielectric losses results are compared. Further, error analyses of all contact-free measurements are performed. Due to a lack of a measure of the specimen deformation by the applied pressure between the electrodes in the contact measurement, error estimation of permittivity determined by IDAX was however not carried out.

The results reveal that the agreements in AWIS measurements are better than estimated errors, though some small deviations are found in harmonic limited waveform results at higher frequencies. Error analysis of the harmonic limited measurement also illustrate that errors are increased with increasing harmonics frequencies. Similar results can be found in figure 4.4. The observed fluctuations of the results with both square-wave and harmonics limited waveforms increase with increasing frequencies. This variation arises from the reduction of the voltage amplitudes of the harmonics that follow the *1/n* dependence. The signal to noise level is thus reduced. As *S/N* ratio decreases with increasing number of harmonics, the useful number of harmonics in the test waveform is limited. However, with the *S/N* ratio of 10^7, AWIS can afford losing some resolution in order to perform harmonic limited dielectric response measurement with contact-free electrode arrangement.
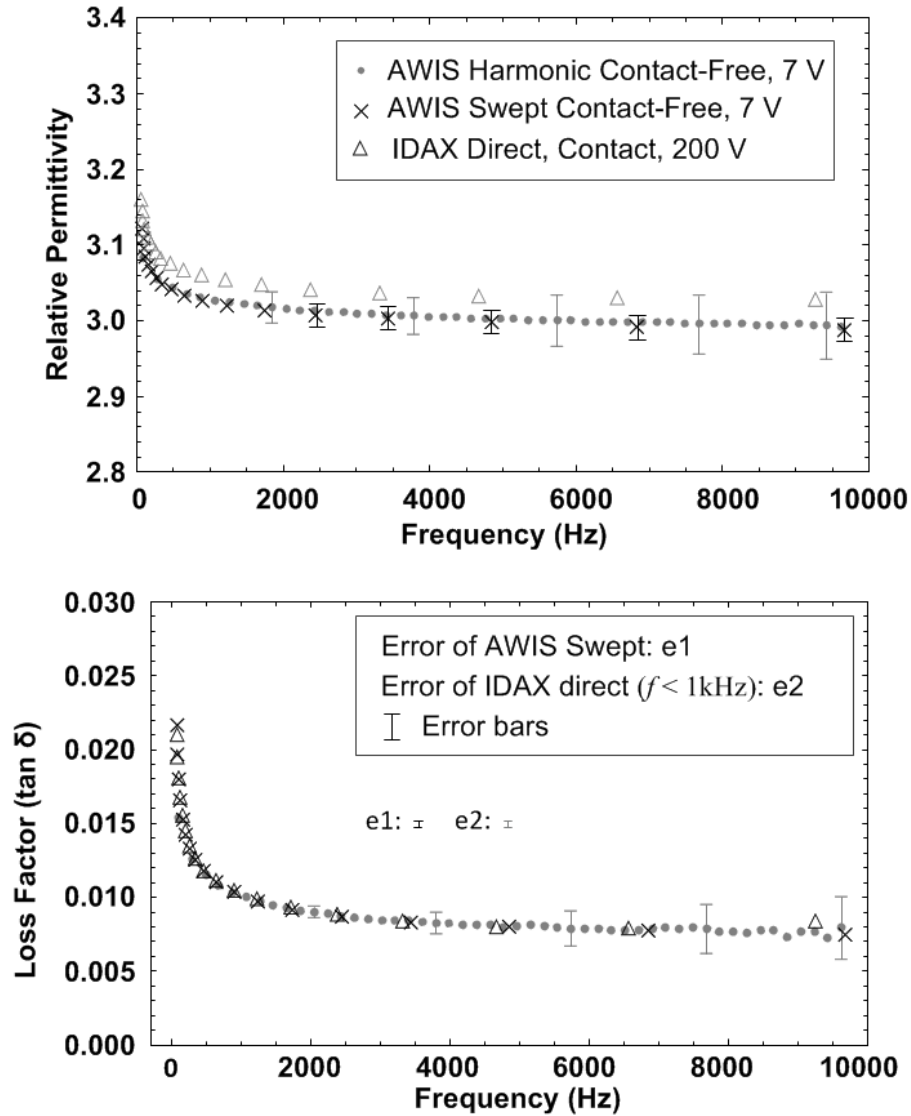
Figure 5.13: Relative permittivity (ε_r) and loss factor (*tanδ*) of 1.92 mm thick EPDM rubber with ATH filler obtained by AWIS with contact-free electrode arrangement and air reference method with harmonic limited waveform (97.2 Hz fundamental frequency, 50 odd harmonics, 16000 samples in the waveform) and swept sinusoidal waveforms. As a reference, a result obtained by IDAX from swept sinusoidal waveforms and contact electrode arrangement is also shown.

5.7 Summary

In this chapter, we have discussed two techniques intended to improve dielectric material characterization, namely air reference method and contact-free electrode arrangement. Further, these two techniques are applied together with harmonic limited waveform for fast dielectric material characterization.

The air reference method can improve instrument accuracy by performing a calibration with a known specimen, air, under the same conditions as the material is tested. Thus, the detailed voltage and current sensing properties are eliminated from the results. This requires that the instrument have the same sensitivity in the reference and the specimen measurements, which is not guaranteed for commercial instruments using automatic sensitivity selection for improving direct measurement accuracy. Our results indicate a substantial improvement in accuracy as compared to direct measurements. In particular, this method may improve loss factor sensitivity into ranges required for characterization of modern insulation materials.

Contact-free measurements are proposed as a solution to the electrode contact problem, which often requires intricate and time-consuming procedures to be under control. To apply a contact-free measurement, the air reference method is required as the dielectric properties of the specimen are found from the ratio of two capacitance measurements. There is inevitably some loss of sensitivity by contact-free measurements as an air gap contribution need to be eliminated from the result. Thus, these measurements demand a higher intrinsic sensitivity than direct measurements whereas they may significantly reduce specimen preparation time and improve reproducibility. The air referencing method eliminates however one important source of error, the sensor calibration error. In cases where this error dominates, an improved accuracy may be obtained despite the loss of accuracy due to the air gap.

The harmonic limited waveforms are used in AWIS technique to perform contact-free measurement with air reference method. The implemented measurement setup enables us to perform fast dielectric material characterization. Though the measurement errors are increased with increasing frequencies due to reduction of harmonic amplitudes, with a high signal to noise ratio, AWIS can afford to lose some resolution in order to perform harmonics dielectric response measurements with contact-free electrode arrangement.

6 Geometric Influence on Permittivity

When the relative permittivity of a dielectric material is calculated from the complex capacitance of a two-electrode fixture, the accuracy of permittivity estimation is often much lower than that of dielectric losses, even though both quantities are determined from the same data set. The reasons are conceivably due to the geometric influences such as specimen thickness, electrode edges and surrounding objects.

In a contact-free electrode arrangement, the precision of permittivity estimation is further reduced due to distance inaccuracies and the presence of an extra air layer. Therefore, the existing edge correction methods may not be suitable for contact-free measurement and new solutions need to be explored.

With the development of modern computer's calculation ability, finite elements models of electrode setups can be implemented and thus the capacitances of models with various configurations can be calculated with high precision at reasonable cost. Compared to a costly manufacturing of a test cell with a precision electrode with guard ring, a finite element model is an attractive alternative to compensate the geometric influences by calculation and it is also valuable in verification of different guard electrode designs that aim for eliminating the geometric effects in precision permittivity determination. Therefore, the use of finite element method for improving the accuracy of permittivity determination is evaluated in this chapter.

Further, a new type of shielding guard ring electrode design is suggested for eliminating the geometric influences from electrode edges and surroundings. The design has been verified by a finite element model. Due to the manufacturing time and cost limitations, the suggested electrode setup is, however, not yet physically implemented.

6.1 Geometric effects

Though the air reference method is suggested to determine dielectric losses with high precision, the geometric influences from the electrode setup still need to be considered as they will decrease the accuracy in permittivity determination. In the air reference measurements, by inserting a specimen into the test gap, the electric field distribution around electrode is changed due to the existence of dielectric interfaces. In addition, as a high impedance shunt is employed in the AWIS system to measure the response current, a non-negligible voltage is generated over the shunt and is present at the electrode. Consequently, the capacitive couplings between electrodes and surrounding objects are introduced, these are further enhanced by presence of electrode supporting materials in-between. As a result, the change of measured capacitance due to the presence of the specimen is reduced and the accuracy of the determined permittivity is decreased accordingly. The geometric influences in permittivity determination are discussed in detail in the following.

6.1.1 Edge effect

The electrode edge effect is the most commonly considered error in permittivity measurements. This effect appears as a result of distortions of electric field lines at electrode edges. It will be further pronounced in contact-free electrode arrangements, as electrostatic flux at electrode edge will curve into the air layer and distort the measured specimen area.

One possible solution to avoid the influence of specimen edge is to measure a specimen which can be totally covered by the electrode. This solution is, however, not so practical, as small specimens require extra care to clean and handle to avoid surface charge interferences in the contact-free measurements. In addition, in the contact electrode arrangement, the edge leakage current might significantly affect measurements on small specimens. Another important factor is that determination of low loss materials (tan $\delta \approx 10^{-4}$) requires sizeable signals to reach a good signal to noise ratio. Using a small specimen, it is difficult to achieve this accuracy level in our present electrode setup. Therefore, the small specimen solution has been abandoned in this study. However, with a better signal to noise ratio and careful handling of specimens, small specimens might still be a good solution for avoiding electrode edge effects in contact-free measurements.

The edge effect is also a well-known issue in determination of the capacitance in two parallel electrode configurations. A usual solution is to use a grounded guard-ring electrode, as illustrated in figure 6.1, which controls the electric field and better defines the effective measurement area. Another advantage of this arrangement is that it prevents undesired surface leakage currents. This solution has been employed in many dielectric studies and is recommended by the IEC standard [1], however, it cannot eliminate the interferences from the shielding box as well as from the guard-ring itself when a non-negligible voltage is generated on the electrode by a high impedance shunt. In the figure, 0.1 V is applied to the bottom measuring electrode to illustrate this effect.

6.1.2 Shielding box

Another inherent error source is the capacitance between electrodes and the grounded shielding box due to the electric field lines which will pass out in all directions. The amount of capacitance increase due to this effect depends on the electrode setup and the voltage potentials on other objects within the box. This effect can further be pronounced in the air reference measurements due to a voltage increase at the measuring electrode when a specimen is measured.

Historically, the shielding box effect has been largely forgotten in determination of dielectric
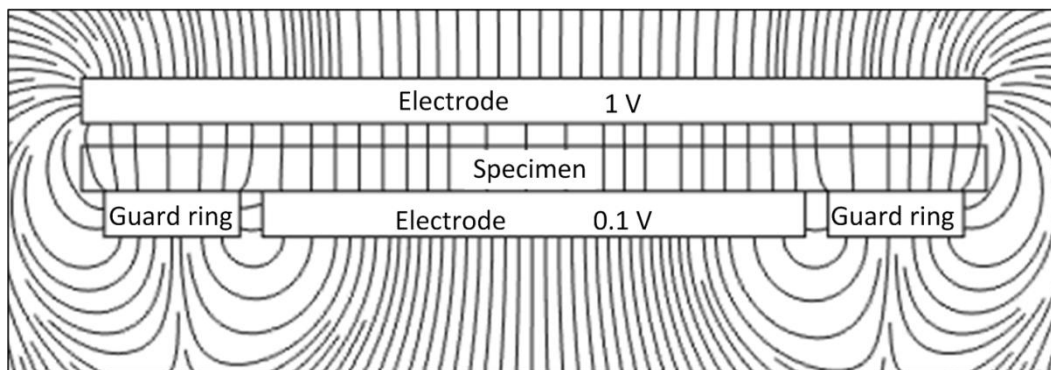

Figue.6.1: Electric field distribution of two parallel disk electrodes with guard ring, the ring electrode is grounded.

permittivity. One reason might be that if an operation amplifier is employed to obtain the dielectric responding current, voltage potential drop over the amplifier is negligible and interferences from the grounded surroundings are therefore insignificant. In applications within high voltage engineering and with interests to obtain a board high-frequency response, a high impedance capacitive shunt is required. Thus, the shielding box needs to be compensated for.

6.1.3 Other influences

As the electric field lines will pass out to all directions to earth from the electrodes when voltage is applied, the measured capacitance will be increased, as discussed above. This capacitance can be even further increased if the flux passes through electrode supporting construction materials, such as glass, wood, plastic, etc. Apart from the supporting materials, connection cables and surrounding objects all add undesired capacitance to the measurement. These interferences cannot be neglected when high precision estimates of permittivity are desired.

In the loss measurements, the increased capacitance due to flux passing entirely through air makes no difference in the dielectric loss current, however, the total capacitance and thereby the loss factor is affected. If this capacitance is partly affected by supporting materials and cable insulations, as is often the case, it may add loss current. In the air reference method, the losses from supporting materials and cables have however been considered as an integral part of the shunt properties and therefore taken care of through the calibration process.

Even though the losses from surroundings are compensated in the air reference method, the reference capacitance is determined only based on the dimension of the test air gap. As the measured total capacitance is larger than the reference capacitance due to the influence of the surroundings, the relative capacitance change due to presence of a specimen in the gap is relatively reduced. As a consequence, the obtained permittivity becomes smaller and a correction is required to improve the accuracy of its determination.

6.2 Correction of geometric influences on permittivity

In this section, two correction methods are described. One is using a finite element model to estimate a geometric correction factor. The other one is using a specially designed shielding guard electrode to eliminate the geometric influences from measurements. Both methods are discussed with a special focus on the application of contact-free electrode arrangement using the air reference method.

6.2.1 FEM-calculation of correction factors

To estimate the correction factors, the same principle as used in the air reference measurement is employed. The detailed FEM model as well as the correction procedure for the air reference measurement is discussed in the following.

6.2.1.1 Finite element model

To compensate for the effects from both electrode edges and surrounding objects, a finite-element model of the used contact-free electrode setup is developed. The model was built in the AC/DC module in the Comsol Multiphysics 4.2a [53] and stationary electrostatic studies were carried out to estimate the capacitances. As the accuracy of FEM calculation is high and models are calculated under ideal conditions, the accuracy of a correction factor is then limited to how
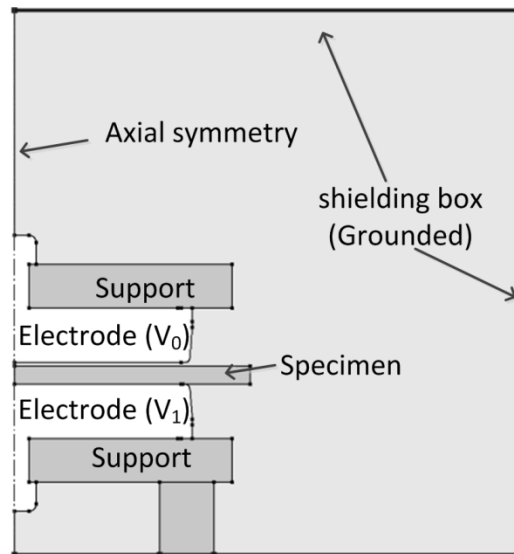
Figure 6.2: 2D symmetric finite element model for geometric influences correction in permittivity determination

complicated a model one can implement. To achieve a high precision, the model might need to be built in 3D with consideration of every fine detail, such as the position of cables. With increasing complexity of model configuration, the model design and computing time will also increase progressively. It was thus decided to limit this study to a 2D configuration at the present stage.

The computational domain of the considered case is illustrated in figure 6.2. The voltage potentials on the electrodes are defined by initial calculations based on a simple circuit model; the shielding box is on ground potential and the properties of the supporting material are also specified. In the model, the test gap distances as well as the thickness of specimen are adjustable. To achieve the highest possible correction accuracy, the 2D model is verified against measurements at different gap distances with air and a good agreement is achieved between simulations and measurements by adjusting the size of shielding box.

6.2.1.2 Calculation of correction factor

The geometric correction factor is obtained from two permittivities, the implemented specimen permittivity in the model and the calculated, "observed", permittivity. To calculate the observed permittivity from the model, the capacitance between the measuring electrode and the rest of the cell is calculated. The accuracy of this calculation depends on potentials assigned to the surrounding objects.

The voltage (V_1) generated at the measuring electrode is calculated based on a simple circuit model, as illustrated in figure 6.3. It consists of three in series connected components, C_{air} is the capacitance of the air gap above specimen and $C_{specimen}$ is specimen capacitance. Both capacitances are calculated assuming the same surface area as the measuring electrode. The applied voltage V_0 and the shunt impedance Z_{shunt} are same as in the measurements. As a result, the calculated voltage potential V_1 is specified for different specimen-electrode dimensions as well as specimen permittivity.
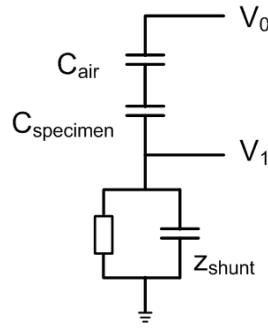
Figure 6.3: Circuit model for calculating generated voltage on the measuring electrode.

In practice, a fixed test gap distance is often desired when comparing different specimens to avoid introducing additional distance uncertainties. This enables combining the test gap distance and the specimen thickness to a distance ratio d_r. The obtained correction factors are, therefore, only applicable for a specified test gap distance.

Once all parameters are implemented in the model, steady-state electrostatics studies are carried out, from which the electrostatic fields as well as electric charges in the model are analyzed. In the finite element model, capacitance can be estimated from equation 6.1, where the V_{10} is the voltage difference between two electrodes (V_1-V_0) and Q is the total surface charge at the measuring electrode.

$$C = \frac{Q}{V_{10}} \tag{6.1}$$

The total surface charge Q is normally calculated by a surface integral of the surface charge density ρ_s at the measuring electrode:

$$Q = \oiint_S \rho_s \, ds \tag{6.2}$$

To calculate a geometric correction factor for the air reference method requires some additional steps. Two capacitances are obtained from the FEM model, with and without a specimen with permittivity (ε_i) between the electrodes. The observed permittivity (ε_m) of the specimen is then obtained from equation 5.6. The ratio of ε_i and ε_m is the geometric correction factor for this specific electrode-specimen arrangement. The same procedure is used to perform additional numerical estimations with different specimen permittivity, specimen thickness, all with their individually estimated voltage on the measuring electrode. The relative permittivity has been varied from 1 to 5 and the distance ratios from filling half the gap ($d_r = 0.5$) to a complete specimen-electrode contact arrangement ($d_r = 1$).

With this data set for a fixed test gap electrode setup, a geometric correction function (δ) is found that is dependent on two parameters: the specimen-gap distance ratio (d_r) and the observed permittivity value (ε_m). The correction function is found by a second-degree polynomial fit to the calculated values and simplifies accurate permittivity determination. After a specimen has been measured by the air reference method, the corrected permittivity is obtained by multiplying the measured permittivity with the correction factor.

6.2.1.3 Results and discussion

It is also valuable to assess how different model parameters, such as electrode voltage potential, shielding box, supporting materials, etc., influence the correction factor. To evaluate it, a reference model is employed, as shown in figure 6.2. The test gap of the reference model is set at 1.4 mm and the specimen thickness is 1 mm. The relative permittivity for the specimen and the supporting material is selected to 3. The applied voltage V_0 at the top electrode is 7 V (the used measuring voltage) and the voltage potentials at the measuring electrode V_1 are set at 0.7 V for the case of air filled capacitor and 1.14 V for the case with inserted specimen To study the influences of different model parameters, changes according the following eight scenarios are made in the model and their corresponding normalized corrections are calculated.

A. Reference model (No change);
B. Voltage potentials on the electrodes are V_0 =7 V, V_1 = 1.14 V for both the cases;
C. Shielding box removed (shielding box boundaries set to zero charge);
D. Size of the shielding box extend by 10%;
E. Size of the shielding box reduced by 20%;
F. No supporting material, calculated by setting the permittivity of supporting material to 1;
G. Size of the support reduced by 10%;
H. Add a cable with ground potential, see figure 6.4.

The normalized corrections of the eight scenarios are compared in figure 6.5. This indicates that the measuring electrode voltage and the presence of a shielding box are the two most influential
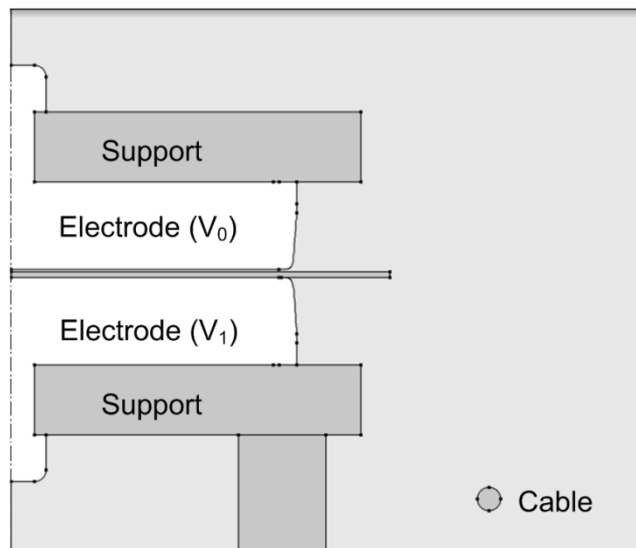

Figure 6.4: FEM model of electrode arrangement with a grounded cable nearby.
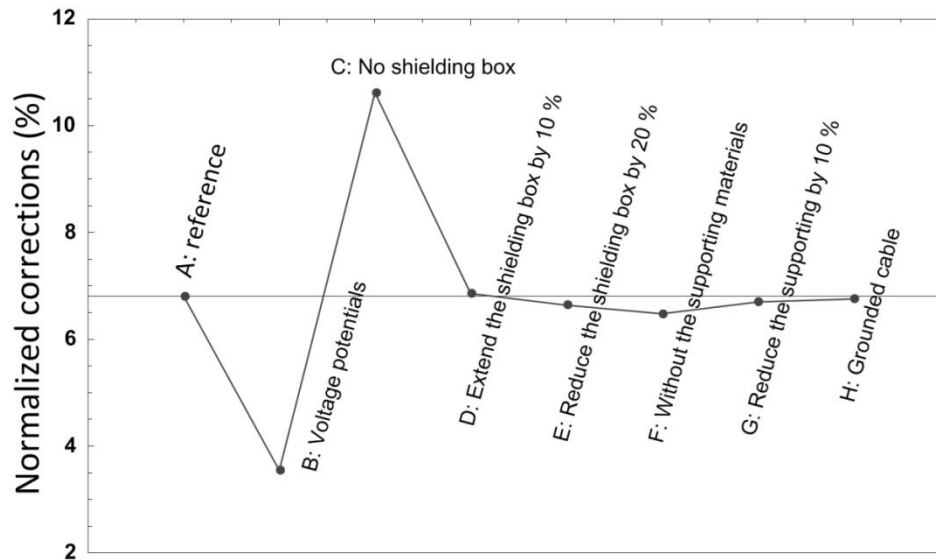
Figure 6.5: Normalized correction factor (%) for eight scenarios considered in the model.

parameters. Thus, if the electrode voltage is not specified in the model, the differences in the two capacitance measurements in the air reference method will not be taken into account and therefore a smaller correction factor is obtained, 3.5% instead for 6.8% for the reference scenario.

If the shielding box is removed, the capacitive coupling between the two electrodes will be enhanced as there is no barrier to block the electric field lines from connecting the backsides of the electrodes. As this gives an increased capacitance, a larger correction is obtained from the calculation.

The other five scenarios have only slight impacts (max 0.37 %) on the correction factor. These scenarios need however to be carefully considered in the model, if a high precision permittivity result is desired. Finally, one should note that almost 7% permittivity correction is required in general (the reference model).

Figure 6.6 shows an estimated geometric correction function for a 1 mm test gap (the electrode arrangement from figure 6.2). The plot indicates that with higher specimen permittivity, a larger correction is required. This is a result of a higher voltage on the measuring electrode and consequently larger influences from the surroundings. Further, the larger permittivity difference between air and the specimen enhance the field distortion at the electrode edge. The plot also shows that, for a constant specimen permittivity, a thin specimen requires more geometric correction than thicker ones. It results from the larger geometric influence of the electrode voltage and the surroundings.

The obtained geometric correction function was applied for permittivity determination of several layers of transparency PET film specimens by the air reference method. The measurements were performed in 1 mm test gap at 1 kHz and 7 V voltage applied. Each film specimen was about 0.1 mm thick.
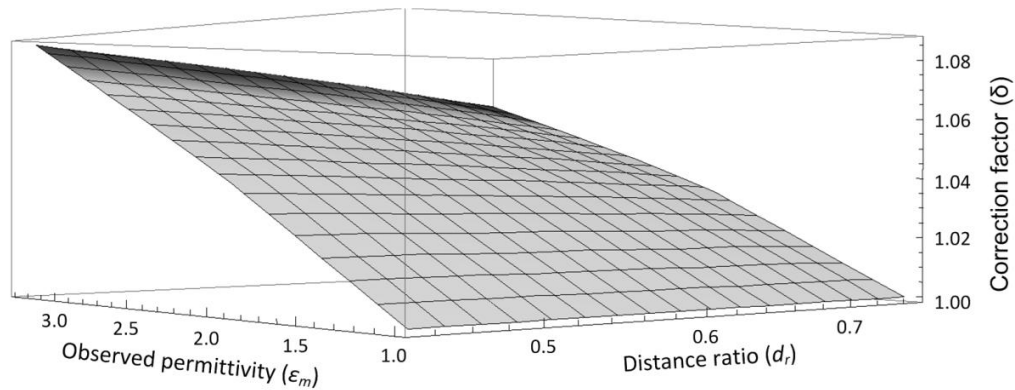
Figure 6.6: The plot of geometric correction factors (δ) for a 1 mm fixed test gap with respect to the observed permittivity (ε_m) and distance ratio (d_r).

The measured and corrected permittivities for different number of layers are shown in figure 6.7. In additional, error estimations were also carried out for both results. For the measured ones, the distance measurement errors as well as the electrical measurement noise and drift errors were considered according to the method discussed in section 5.4.2. Whereas, in the corrected results, an additional error of $\pm 0.37\%$ due to the geometric correction factor was added.

As show in figure 6.7, all the corrected results are about 7% larger than the measured permittivity values. The corrected results are expected to be constant, however a slope is still observed with increasing number of specimens, though the slope is smaller than the slope of the directly

Figure 6.7: Measured and corrected permittivity of several layers of PET film specimens (about 0.1 mm each) in 1 mm fixed test gap, the applied voltage for all the measurements were 1 kHz and 7 V.

measured results and it is within half of the estimated error range. With increasing number of layers, a higher permittivity values is obtained. The reason could be t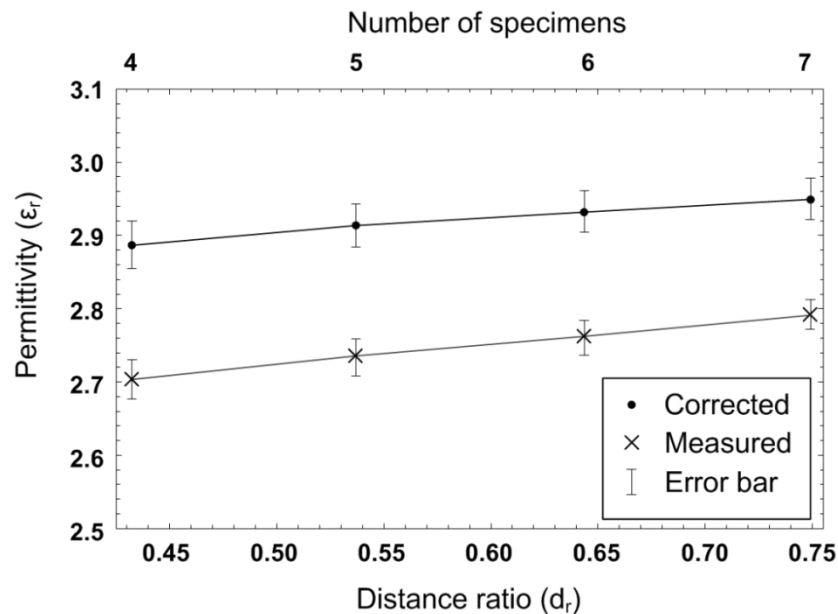hat the slope in permittivity dependence indicate that the model is yet not enough precise to compensate for all geometric influences. This might be because of the limitations forced by 2D approach, where parts in the physical set-up, such as cables, connectors and supporting screws are neglected. Nevertheless, the corrected permittivity should now be correct to the 2nd digit. From the sensitivity estimate in figure 6.5, we estimate that this is the best accuracy one reasonably can achieve with moderately complicated 2D calculations.

6.2.2 Shielding guard electrode

Instead of using a model calculation to compensate the geometric influences, another solution is to eliminate the geometric influences directly in the measurement setup. A guard ring electrode is a typical example. However, the drawback of this technique is obvious, with a grounded guard ring electrode close to the measuring electrode, the measured capacitance is significantly increased and the interference from grounded surroundings still exist as they are coupled to the bottom of the measuring electrode. To eliminate these interferences, a shielding guard electrode is suggested. Due to time constraints and the cost of high precision manufacturing, the suggested setup is however not realized in this work and thus only a design verification by the simulation model can be presented here.

To limit the electrode edge effect, the guard ring concept is inherited by the shielding guard electrode. However, to avoid capacitive coupling between the measuring electrode and the guard electrode, the voltage on both electrodes need to be identical. As there is no voltage difference, the gap between two electrodes can be designed as small as electrically and mechanically possible. This is favorable because the gap distance is a remaining error of the design. Further, to avoid interferences from shielding box and surroundings, the measuring electrode need to be covered by the shielding guard electrode on the backside as well.

A drawing of a shielding guard electrode is shown in figure 6.8. To achieve the same voltage on both the shielding guard and measuring electrode, the size of the shielding electrode can be adjusted to have same impedance to the high voltage electrode as the measuring electrode. If then
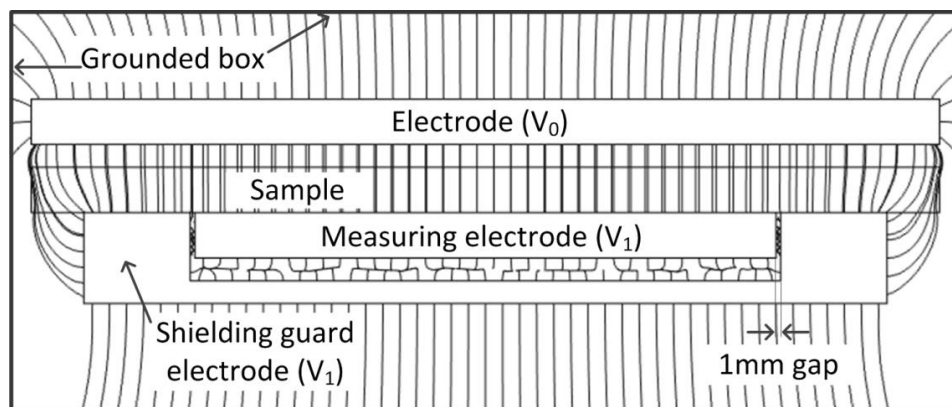

Figue.6.8: Electric field distribution of two parallel disk electrodes with shielding guard electrode. The voltage potentials generated at measuring electrode and the shielding guard electrode are expected to be the same.

the shielding electrode is connected through a shunt with the same impedance as the current measurement shunt, the two electrodes will automatically have the same potential.

6.2.2.1 Simulation model

To verify the design of the shielding guard electrode, FEM calculation is employed again and two other traditional guard ring electrode setups are additionally studied as references.

All three models were implemented in the AC/DC module of Comsol Multiphysics 4.2a [53] in a 2D geometry. The geometry of the shielding guard electrode setup is shown in figure 6.8. The other two references models have an identical electrode configuration as illustrated in figure 6.1.

The difference between the two reference models is the voltage on the guard ring. One guard ring is at ground potential and the other one has the same potential as the measuring electrode. All three models have a fixed test gap of 15 mm and the distance between measuring electrode and guard is 1 mm. Two specimen dimensions (10 mm and 14 mm in thickness) combined with three different permittivity values (2, 3, 4) were used in all three models for permittivity calculations.

The applied voltage on the high voltage electrodes of all models are the same, $V_0 = 10$ V, and the voltage, V_1, on the measuring electrode with different specimen parameters are calculated according to the simple circuit model illustrated in figure 6.3. The voltage on the shielding guard electrode and one guard ring electrode are the same as the calculated V_1.

To calculate the "measured" permittivity from the different specimen-electrode arrangements, the capacitances of the model were first estimated from the measuring electrode, then, the air reference method was applied to obtain the permittivity from the capacitances.

6.2.2.2 Result and discussion

The calculated "measured" permittivity from the three electrode models with different specimen properties are listed in table 6.1. The results show that the shielding guard electrode gives the permittivity closest to the ideal. The results of the other two guard ring configurations indicate that voltages on the adjacent objects can largely influence the measurement accuracy. To further compare the accuracy of different electrode arrangements, the relative error ranges of "measured" permittivity are plotted in figure 6.9.

As indicated in figure 6.9, the shielding guard electrode results have negligible error in all the calculations, whereas the other two guard ring arrangements have much higher errors. The plots show that the errors increase with increasing value of permittivity and decreasing value of d_r. Similar variations are found in the normalized sensitivity parameters of electrical measurement error in the air reference method as shown in figure 5.7.

The highest error range is found from the grounded guard ring arrangement and this error level is about the same as the errors obtained from the "bare" electrode setup, which is illustrated in figure 6.2 and figure 6.6. The comparable error levels indicate that a guard ring electrode at ground potential is not sufficient to improve the accuracy of permittivity determination. To substantially increase the accuracy, shielding of the measuring electrode and the voltage on the guard electrode are the two important factors to consider.

In this study, we have however, neglected the difficult aspect of how to generate an identical voltage on both the measuring and guard electrodes in practice. To achieve this, the test gap, the size of both electrodes and the surrounding shielding box might need to be fixed. Further, the

specimen size also needs to be well defined. This is because all the factors above will have geometric influences on the shielding guard electrode. An alternative solution might be to have an external voltage supply connected to the shielding guard electrode, from which the voltage can be adjusted according to the voltage level at the measuring electrode. The suggested solutions should be subject of further studies.

Table 6.1: Calculated permittivity from applying the air reference method in the three different electrode arrangements models. The guard ring electrode is illustrated in figure 6.1; shielding guard ring electrode is shown in figure 6.8 and voltage V_1 is the voltage potential on the measuring electrode. The test gap distance is fixed to 15 mm for all electrodes and the gap between guard and measuring electrode is 1 mm.

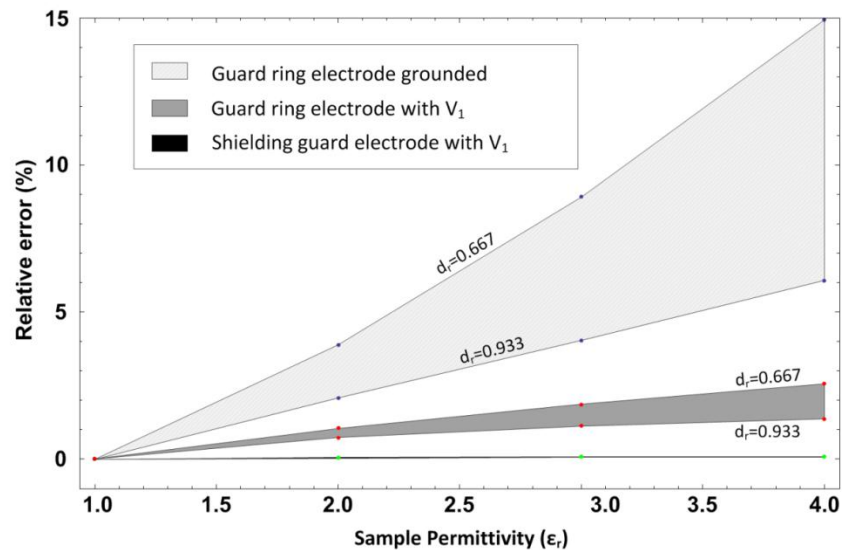| Ideal ε_r	2	3	4
d_r	**Grounded guard ring electrode**		
0.667	1.92234	2.7323	3.40186
0.933	1.95828	2.87915	3.75661
	Guard ring electrode with V_1		
0.667	1.97856	2.94384	3.89683
0.933	1.98512	2.96637	3.94491
	Shielding guard electrode with V_1		
0.667	1.99867	2.99721	3.99592
0.933	1.99901	2.99786	3.99668

Figure 6.9: Relative error of the calculated "measured" permittivity that listed in table 6.1.

6.3 Summary

In this chapter we have discussed the two methods that aim for improving the accuracy of dielectric permittivity determination by either compensating or shielding the interferences from electrode test set-up.

In dielectric material characterization, permittivities are often determined from a two-electrode fixture and therefore subject to electrode edge effect. This is handled by applying a guard ring electrode in most conventional approaches. Further studies indicated that not only the electrode edge but also the shielding box and other parts of the surroundings have influences on the permittivity accuracy, if a non-negligible voltage is presented at the measuring electrode. This might not be the case when the response currents are measured through a current amplifier. However, a high impedance current shunt, which inevitably leaves some voltage on the measuring electrode, is desired in our high voltage applications that requires high frequencies.

The geometric correction derived from finite element model calculations provides one possible way to increase the accuracy of permittivity by an order of magnitude, provided that the voltage on the measurement electrode is accounted for. This has been verified even for electrode systems without guard ring.

Through the study of finite element method compensation, a shielding guard electrode system has been conceived. In contrast to ordinary guard rings, it can eliminate the need for the geometric corrections. It is however required that the shielding guard has the same potential as the measuring electrode and that it shields the backside of the measuring electrode.

This study provides a few alternatives to the current amplifier sensing; therefore it may be valuable for dielectric material characterization as it can enable fast dielectric studies in a higher frequency range.

7   Conclusions

The main objective of the work present in this thesis was to enhance dielectric response characterization of solid insulation materials. To achieve this aim, the research activities were concentrated on two main aspects. One was related to the measurement time and the other was focused on the measurement accuracy. Both aspects are complementary to each other. Using the AWIS technique and the finite element method, the aim was achieved as described in the previous chapters and the conclusions of this work are presented below.

7.1   Fast dielectric characterization

Harmonic limited waveforms and contact-free electrode arrangements are implemented in this work to enable fast dielectric response measurements.

Signals with high harmonic content can be used by the AWIS technique to determine a wide dielectric frequency response spectrum from one measurement. However, too high harmonic content will limit the measurement accuracy due to aliasing. To avoid signal aliasing, the harmonics limited waveform must be generated considering the fundamental frequency, the number of samples in the waveform and the sampling rate in the measurement. This was facilitated by the equations for the apparent frequencies of aliased signals. With a frequency spectrum determined from one measurement, the optimized test waveforms enable all the frequencies responses to be determined under identical test conditions and possible systematic errors in the frequency response are eliminated.

Specimen preparation procedures in solid dielectric characterization are often time-consuming and complicated. Any poor surface contact between specimen and electrode will result in a significant increase in loss at high frequency due to series connected surface resistance. Further, in contact specimen-electrode arrangement, the applied pressure from electrodes may deform the specimen and influence the accuracy of the determined permittivity. Contact-free electrode arrangement was therefore suggested in this work to avoid elaborate specimen preparation and increase the measurement accuracy.

The combination of harmonic limited waveforms and contact-free electrode arrangements enable the use of AWIS for fast dielectric characterization and study of dielectric materials under rapidly changing environmental conditions.

7.2   Accuracy improvement

To improve the accuracy of measurement, the work was first focused on optimization of AWIS setup. A measurement noise level around ppm was achieved by implementing a shielding box, a voltage supply with batteries and proper grounding. With additional help of a voltage divider, a voltage follower as well as separation channels, crosstalk interferences were largely reduced down to the noise level.

Further, the accuracy of the dielectric response parameters, loss factor and permittivity, are improved in this work by implementing an air reference method and considering the geometric influence in the electrode setup.

The air reference method was demonstrated in this work to improve instrument accuracy by performing a calibration with a known medium, air, under the same conditions as the dielectric is tested. Thus, the detailed voltage and current sensing properties are eliminated from the results. This requires that the instrument have the same sensitivity in the reference and the specimen measurements. The experimental results indicate a substantial improvement in accuracy as compared to direct measurements. In particular, this method may improve loss factor sensitivity into ranges required for characterization of modern insulation materials.

To apply a contact-free measurement, the air reference method is required as the dielectric properties of the specimen are found from the ratio of two capacitance measurements. There is inevitably some loss of sensitivity as an air gap contribution need to be eliminated from the result whereas this method may significantly reduce specimen preparation time and improve reproducibility. The air referencing method eliminates one important source of error, the sensor calibration error. In cases where this error dominates, an improved accuracy may be obtained despite the loss of accuracy due to the air gap.

Permittivities are often determined from the capacitance of a two-electrode fixture, therefore electrode edge, shielding box, and other parts of the surroundings will have influence on the accuracy if a non-negligible voltage is generated at the measuring electrode over a high impedance current shunt. Two methods to either compensate or shield the interferences from electrode test set-up were discussed in this work to improve the accuracy of dielectric permittivity.

The geometric correction derived from finite element model calculations provides one possible way to increase the accuracy of permittivity by an order of magnitude, provided that the voltage on the measurement electrode is accounted for.

By the study of finite element compensation, a shielding guard electrode system has been conceived. In contrast to ordinary guard rings, it can eliminate the need for the geometric corrections. It is however required that the shielding guard has the same potential as the measuring electrode and that it shields the backside of the measuring electrode.

The correction of geometric influences provides a few alternatives to the commonly used current amplifier sensing. Thus, it may be valuable for dielectric material characterization as it can enable fast dielectric studies at a higher frequency range.

8 Future Work

In this thesis some enhancements of dielectric response characterization using the AWIS technique has been found. Therefore, the most natural continuation of the work is to refine the measurement setup and make it more user-friendly.

One direction of the refining work is on the electrode setup. Electrodes can be implemented as a vertical setup with two guard rings, which will hold a specimen between two parallel electrodes with both specimen surfaces contact-free. As mentioned in the thesis, a shielding guard electrode setup might be valuable in practice and therefore some work related to voltage adjustment of the shielding electrode is required.

It would be interesting to study measurements with small specimens as these may help to avoid electrode edge effect but not the other geometrical corrections. Further, more studies regarding FEM correction of geometric influences might be fruitful for a more practical use of permittivity measurements.

In this thesis, all the measurements were performed at relatively low voltages, it is therefore desirable to refine the whole test setup and apply it in high voltage experiments. This work may study the current from partial discharges in addition to the dielectric current and thus investigate the material degradation process under partial discharges.

9 References

[1]   Recommended methods for the determination of the permittivity and dielectric dissipation factor of electrical insulating materials at power, audio frequency including metre wavelengths, IEC 250, 1969.

[2]   E.T.Hoch, "Electrode effects in the measurement of power factor and dielectric constant of sheet insulating materials," Bell System Tech. Jour., vol. 5, pp. 555-572c, Oct. 1926.

[3]   A. H. Scott and H. L. Curtis, "Edge correction in the determination of dielectric constant," Journal of Research of the National Bureau of Standards, vol. 22, p. 23, 1939.

[4]   B. Sonerud, "Characterization of Electrical Insulation Exposed to Arbitrary Voltage Waveforms," Doctoral Thesis, Department of materials and manufacturing technology, Chalmers University of Technology, Göteborg, 2010.

[5]   B. Sonerud, T. Bengtsson, J. Blennow, and S. M. Gubanski, "Dielectric response measurements utilizing non-sinusoidal waveforms," in Electrical Insulation and Dielectric Phenomena, 2006 IEEE Conference on, pp. 43-46, 2006.

[6]   B. Sonerud, T. Bengtsson, J. Blennow, and S. M. Gubanski, "Dielectric response measurements utilizing semi-square voltage waveforms," Dielectrics and Electrical Insulation, IEEE Transactions on, vol. 15, pp. 920-926, 2008.

[7]   A. K. Jonscher, *Dielectric relaxation in solids*. London Chelsea Dielectrics Press Ltd., 1983.

[8]   W. S. Zaengl, "Dielectric spectroscopy in time and frequency domain for HV power equipment. I. Theoretical considerations," IEEE Electr. Insul. Mag., vol. 19, pp. 5-19, 2003.

[9]   U. Gafvert, L. Adeen, M. Tapper, P. Ghasemi, and B. Jonsson, "Dielectric spectroscopy in time and frequency domain applied to diagnostics of power transformers," in IEEE Int'l Conf. Properties and Applications of Dielectric Materials, Xi'an China, pp. 825-830 vol.2, 2000.

[10]   J. Blennow, C. Ekanayake, K. Walczak, B. Garcia, and S. M. Gubanski, "Field experiences with measurements of dielectric response in frequency domain for power transformer diagnostics," IEEE Trans. Power Delivery, vol. 21, pp. 681-688, 2006.

[11]   S. M. Gubanski, P. Boss, G. Csépes, V. Der Houhanessian, J. Filippini, P. Guuinic, U. Gäfvert, V. Karius, J. Lapworth, G. Urbani, P. Werelius, and W. Zaengl, "Dielectric response methods for diagnostics of power transformers," IEEE Electr. Insul. Mag., vol. 19, pp. 12-18, 2003.

[12]   B. Oyegoke, P. Hyvonen, M. Aro, and G. Ning, "Application of dielectric response measurement on power cable systems," IEEE Trans. Dielectr. Electr. Insul., vol. 10, pp. 862-873, 2003.

[13]   W. S. Zaengl, "Applications of dielectric spectroscopy in time and frequency domain for HV power equipment," IEEE Electr. Insul. Mag., vol. 19, pp. 9-22, 2003.

[14]   P. Werelius, P. Tharning, R. Eriksson, B. Holmgren, and U. Gafvert, "Dielectric spectroscopy for diagnosis of water tree deterioration in XLPE cables," IEEE Trans. Dielectr. Electr. Insul., vol. 8, pp. 27-42, 2001.

[15]   *Insulation Diagnostics Spectrometer "IDA 200"*. Manufactured by PROGRAMMA Electric AB, Täby, Sweden.

[16]   D. Belega, D. Dallet, and D. Petri, "Accuracy of Sine Wave Frequency Estimation by Multipoint Interpolated DFT Approach," Instrumentation and Measurement, IEEE Transactions on, vol. 59, pp. 2808-2815, 2010.

[17]   T. Grandke, "Interpolation Algorithms for Discrete Fourier Transforms of Weighted Signals," Instrumentation and Measurement, IEEE Transactions on, vol. 32, pp. 350-355, 1983.

[18]   C. Kui Fu and M. Shu Li, "Composite Interpolated Fast Fourier Transform With the Hanning Window," Instrumentation and Measurement, IEEE Transactions on, vol. 59, pp. 1571-1579, 2010.

[19]   C. Offelli and D. Petri, "Interpolation techniques for real-time multifrequency waveform analysis," IEEE Trans. on Inst. and Meas., vol. 39, pp. 106-111, 1990.

[20]   H. Renders, J. Schoukens, and G. Vilain, "High-Accuracy Spectrum Analysis of Sampled Discrete Frequency Signals by Analytical Leakage Compensation," Instrumentation and Measurement, IEEE Transactions on, vol. 33, pp. 287-292, 1984.

[21]   B. Sonerud, T. Bengtsson, J. Blennow, and S. M. Gubanski, "Noise and Aliasing Aspects in a Multiharmonic-Dielectric-Response-Measurement System," Instrumentation and Measurement, IEEE Transactions on, vol. 60, pp. 3875-3882, 2011.

[22]   J. Hedberg and T. Bengtsson, "Straight Dielectric Response Measurements with High Precision," presented at the Nord-IS 05, Trondheim, Norway, 2005.

[23]   *IDAX User's Manual*: Megger AB, 2009

[24]   M. Koch, M. Krueger, and M. Puette, "Advanced Insulation Diagnostic by Dielectric Spectroscopy," OMICRON2011.

[25]   W. P. Baker and F. B. Waddington, "Dielectric measurements on thin films by means of electrodes coated with irradiated silicone rubber," J. Sci. Instrum., vol. 36, pp. 309-312, 1959.

[26]   A. Castro-Couceiro, M. Sánchez-Andújar, B. Rivas-Murias, J. Mira, J. Rivas, and M. A. Señarís-Rodríguez, "Dielectric response in the charge-ordered Ca2-xPrxMnO4 phases," Solid State Sciences, vol. 7, pp. 905-911, 2005.

[27]   H. Provencher, B. Noirhomme, and E. David, "Effect of aging on the dielectric properties of insulation paper of power transformers," in IEEE Conf. Electrical Insulation (EIC), pp. 473-477, 2009.

[28]   J. Mijovic, J. Kenny, A. Maffezzoli, A. Trivisano, F. Bellucci, and L. Nicolais, "The principles of dielectric measurements for in situ monitoring of composite processing," Composites Science and Technology, vol. 49, pp. 277-290, 1993.

[29]   A. Campbell, "On the Electric Inductive Capacites of Dry Paper and of Solid Cellulose," Proceedings of the Royal Society vol. 78, p. 196, 1906.

[30]   X. Hairu, Z. Yewen, and Z. Feihu, "Study on measuring method of dielectric spectroscopy for polymer dielectrics," in IEEE 9th Int'l Conf. Properties and Applications of Dielectric Materials (ICPADM) pp. 922-925, 2009.

[31]   A. C. Lynch, "Edge capacitance in the measurement of dielectric properties," Electrical Engineers, Proceedings of the Institution of, vol. 120, pp. 934-938, 1973.

[32]   L. Hartshorn, W. H. Ward, B. A. Sharpe, and B. J. O'Kane, "The effects of electrodes on measurements of permittivity and power factor on insulating materials in sheet form," Electrical Engineers, Journal of the Institution of, vol. 75, pp. 730-736, 1934.

[33]   D. G. W. Goad and H. J. Wintle, "Capacitance corrections for guard gaps," Meas. Sci. Technol., vol. 1, p. 965, 1990.

[34]   D. E. Woolley, "Edge Correction in Calculation of Dielectric Constant," Journal of Testing and Evaluation, vol. 39, pp. 140-149, Mar 2011.

[35]   G. Kirchhoff, "Zur Theorie des Condensators," Monatsberichte der Königlich Preussischen Akademie der Wissenschaften zu Berlin, pp. 144-162, 1877.

[36]   H. J. Wintle, "Capacitance corrections for the guard, edge and corner situations," in Electrical Insulation, 1990., Conference Record of the 1990 IEEE International Symposium on, pp. 435-438, 1990.

[37] H. J. Wintle and S. Kurylowicz, "Edge Corrections for Strip and Disc Capacitors," Instrumentation and Measurement, IEEE Transactions on, vol. 34, pp. 41-47, 1985.

[38] ASTM D150 - 11 Standard Test Methods for AC Loss Characteristics and Permittivity (Dielectric Constant) of Solid Electrical Insulation, ASTM International, 1998.

[39] M. Kaufhold, H. Aninger, M. Berth, J. Speck, and M. Eberhardt, "Electrical stress and failure mechanism of the winding insulation in PWM-inverter-fed low-voltage induction motors," Industrial Electronics, IEEE Transactions on, vol. 47, pp. 396-402, 2000.

[40] L. Paulsson, B. Ekehov, S. Halen, T. Larsson, L. Palmqvist, A. A. Edris, D. Kidd, A. J. F. Keri, and B. Mehraban, "High-frequency impacts in a converter-based back-to-back tie; the Eagle Pass installation," Power Delivery, IEEE Transactions on, vol. 18, pp. 1410-1415, 2003.

[41] B. Sonerud, T. Bengtsson, J. Blennow, S. M. Gubanski, and S. Nilsson, "Capacitance measurements and tree length estimation during electrical treeing in sub-picofarad samples," Dielectrics and Electrical Insulation, IEEE Transactions on, vol. 16, pp. 1707-1709, 2009.

[42] B. Sonerud, J. Blennow, S. M. Gubanski, S. Nilsson, and T. Bengtsson, "Continuous monitoring of dielectric properties of LDPE samples during electrical treeing," in Solid Dielectrics (ICSD), 2010 10th IEEE International Conference on, pp. 1-4, 2010.

[43] B. Sonerud, T. Bengtsson, J. Blennow, and S. M. Gubanski, "Measurement and analysis of partial discharge current during square voltage waveforms," presented at the Electrical Insulation and Dielectric Phenomena, 2009. CEIDP '09. IEEE Conference on, 2009.

[44] "OP-42GP datasheet," ed: Analog Devices.

[45] "Simultaneous Sampling Data Acquisition Architectures," ed: National Instruments Corporation, 2009.

[46] "User's Guide HP 33120A Function Generator / Arbitrary Waveform Generator," ed: Hewlett-Packard Company, 1997.

[47] U. Grenander, *Probability and statistics: the Harald Cramér volume*: Almqvist & Wiksell, 1959.

[48] A. Tanaka, K. Tohyama, T. Tokoro, M. Kosaki, and M. Nagao, "High field dissipation current waveform of polyethylene film obtained by new method," in Electrical Insulation and Dielectric Phenomena, 2002 Annual Report Conference on, pp. 610-613, 2002.

[49] S. Tsuboi, K. Tohyama, and M. Nagao, "Film Thickness Dependence of Dissipation Current for LDPE Film under Trapezoid Waveform Application," in Electrical Insulation and Dielectric Phenomena, 2006 IEEE Conference on, pp. 210-213, 2006.

[50] L. G. Hector and H. L. Schultz, "The Dielectric Constant of Air at Radiofrequencies," Physics, vol. 7, pp. 133-136, 1936.

[51] *Production data sheet Makrolon GP Soild ploycarbonate sheet*, October 2004.

[52] Veeco, *Dektak 6M Manual*. California Digital Instruments Veeco Metrology Group, 2002.

[53] Comsol, *AC/DC Module user's guide*, Version 4.2a ed., 2011.